NTNU – Trondheim
Norwegian University of
Science and Technology

Integrating Offshore Wind Power and Multiple Oil and Gas Platforms to the Onshore Power Grid using VSC-HVDC Technology

Magne Lorentzen Kolstad

Master of Science in Electric Power Engineering
Submission date: June 2013
Supervisor: Tore Marvin Undeland, ELKRAFT

Norwegian University of Science and Technology
Department of Electric Power Engineering

Problem description

The oil and gas industry are responsible for about 25 % of the total greenhouse gas emissions from Norway. Most of these emissions are due to energy production. Today most of the offshore oil and gas platforms get there energy from gas fired turbines located on the platforms. These turbines have efficiency between 30 % - 40 % and are the major source of emissions from the Norwegian continental shelf. By replacing the energy from the gas turbines with renewable energy from offshore wind farms and hydro power from the onshore power grid the total greenhouse gas emissions from Norway can be greatly reduced.

A system consisting of five oil and gas platforms and one offshore wind farm connected to the onshore power grid through a common High Voltage Direct Current (HVDC) transmission system based on Voltage Source Converters (VSC) are to be studied. The feasibility of the system should be evaluated based on simulations. The following tasks should be included in this master thesis:

- Develop a dynamic simulation model of the system using SimPowerSystems in MATLAB®/Simulink®.
- Develop a control strategy and a VSC control system.
- Run simulations and study the dynamic behavior of the system during sudden variations in the load including: disconnection of the wind farm, load shedding, and large motor start up.
- Interpret and discuss the simulation results based on the grid code regarding offshore power systems and the simplification done in the model.

Preface

This report is the result of my final semester at the Norwegian University of Science and Technology (NTNU) and represents the end of my 2 year master program in Electric Power Engineering.

During this project I have been fortunate to have been surrounded with people who have shown great interest in my work and were willing to assist me. This semester has been very educational and it has been a pleasure and truly inspiring to work with people who has been so enthusiastic about this subject. Special thanks go to Atle Rygg Årdal at SINTEF Energy Research for the numerous hours he has spent on my thesis. His help with getting the simulation model up and running was very valuable. I am also extremely grateful for his help with analyzing the simulation results and with proof reading the report. I would also like to thank my co-supervisor, Dr. Eng. Kamran Sharifabadi in Staoil. He initiated the project and has been helpful with supplying literature and simulation parameters throughout the project. Finally I would like to thank my supervisor Prof. Tore M. Undland for the opportunity to explore the field of power electronics and for his guidance and helpful comments along the way.

Abstract

This thesis investigates the possibilities of integrating oil and gas platforms and offshore wind power to the onshore power grid. The main motivation for this is to reduce the large greenhouse gas emissions associated with traditional oil and gas platforms. The oil and gas industry is responsible for 25 % of total greenhouse gas emissions from Norway. The major part of these emissions originates from the power generation on the platforms. By supplying the oil and gas platforms with renewable energy from the onshore power grid in combination with offshore wind power there will be little or no use for power generation on the platforms and greenhouse gas emissions can be greatly reduced.

The feasibility of a hypothetical power system in the North Sea consisting of five oil and gas platforms and one offshore wind farm with a common connection to the onshore power grid is studied. The connection to the onshore grid is realized through a High Voltage Direct Current (HVDC) transmissions system based on Voltage Source Converter (VSC) technology The main goal of this thesis is to gain understanding of the system dynamics and the control of VSC-HVDC transmission system, offshore wind power, as well as offshore power systems.

A dynamic simulation model of the system and a control system has been developed using SimPowerSystems in MATLAB®/Simulink. In order to save computation time aggregated models are used. The load on the platforms consists of a passive load, a fixed speed induction motor, and a constant power load representing variable speed drives on the platform. The wind farm consists of a wind turbine and a permanent magnet synchronous machine operating at variable speed using a back-to-back VSC. The converters in the VSC-HVSC transmission system and the wind farm are modeled using average models. Simulations are performed on system disturbances that are thought to be critical for the operation of the system. The simulation cases represent large and partly exaggerated disturbances in order to test the limitations of the system.

The simulation results showed that the developed control system was able to keep the voltage and frequency variations within the grid code in IEC 61892 even during large disturbances. It was concluded that the system handles variations in the load very well and that the system configuration studied in this thesis is regarded as a feasible way of integrating oil and gas platforms and offshore wind power to the onshore grid. However more detailed studies are recommended including short circuit analysis.

Sammendrag

Denne avhandlingen undersøker muligheten for å integrere olje- og gassplattformer og offshore vindkraft med kraftnettet på land. Hovedmotivasjonen bak dette er å redusere de store klimagassutslippene forbundet med tradisjonelle olje- og gassplattformer. Olje- og gassindustrien står for 25 % av de totale klimagassutslippene i Norge. Hoveddelen av disse utslippene stammer fra kraftproduksjon på plattformene. Ved å forsyne olje- og gassplattformer med fornybar energi fra kraftnettet på land i kombinasjon med offshore vindkraft vil det være lite eller ingen bruk for kraftproduksjon på plattformene og klimagassutslippene vil kunne bli sterkt redusert.

Denne oppgaven er en mulighetsstudie av et tenkt kraftsystem i Nordsjøen bestående av fem olje- og gassplattformer og en offshore vindpark med en felles tilkobling til kraftnettet på land. Tilkoblingen til land er realisert ved hjelp av et HVDC overføringssystem basert på Voltage Source Converter (VSC) teknologi. Hovedformålet med denne oppgaven er å gi økt forståelse for dynamikken i systemet, samt kontroll av VSC-HVDC overføringssystem og offshore vindparker.

En dynamisk simuleringsmodell av systemet og et kontrollsystem er utviklet i SimPowerSystems i MATLAB®/Simulink. For å redusere beregningstiden er det benyttet aggregerte modeller. Lasten på plattformene er modellert som en passiv last, en induksjonsmotor og en konstant effekt last for å representere motordriftene på plattformen. Vindpark modellen består av en vindturbin og en permanentmagnet synkrongenerator som opererer med variabel hastighet ved hjelp an en back-to-back VSC. Omformerne i VSC-HVDC overføringssystemet og i vindparken er modellert ved hjelp av gjennomsnittsmodeller. Simuleringer av systemet har blitt utført for forstyrrelser som er antatt å være kritisk for driften av systemet. Forstyrrelsene er store og til dels overdrevne for å teste begrensningene til systemet.

Resultatene av simuleringene viste at kontrollsystemet var i stand til å holde variasjonen i spenningen og frekvensen innenfor grensene gitt i IEC61892 selv under store forstyrrelser. Det ble konkludert med at systemet håndterer variasjoner i lasten bra og at systemkonfigurasjonen studert i denne rapporten er en mulig måte å integrere olje- og gassplattformer og offshore vindkart i kraftnettet på land. Mer detaljerte studier, inkludert kortslutningsberegninger, er anbefalt.

Table of Contents

Table of figures

1 Introduction

1.1 Background and motivation

Norway has committed to reduce the global greenhouse gas emissions by 30 % compared to their own emissions in 1990, within 2020 [1]. About two-thirds of the cuts are to be made nationally. Numbers from 2012 show that Norway actually has increased total greenhouse gas emission by over 5 %, compared to 1990 [2]. The main reason for this is an increase in the emissions from the oil and gas industry with over 75 %. Today the oil and gas industry is responsible for more than 25 % of the emissions from Norway. If Norway is going to reach their ambitious climate goals, alternative power generation and supply solutions have to be considered. Today most oil and gas platforms are self supplied with electrical energy from gas fired turbines located on the platforms. These turbines typically have efficiency between 30 % - 40 % [3] and are the major source of emissions from the Norwegian continental shelf [4]. The Norwegian continental shelf is also facing some challenges in the oncoming years that will lead to an increased energy demand. This is mainly [5]:

- Measures to increase reserves from mature fields, including water and gas injection.
- Reduction of reservoir pressure, which requires additional compression force.
- Increased water production from aging fields.
- Transition from primarily oil production to a larger share of gas production and transport of gas.

The installed power per produced petroleum unit is therefore expected to grow in the oncoming years. This will lead to further increase in greenhouse gas emissions if not measures are taken. By replacing the energy from the gas turbines with energy from renewable sources Norway's greenhouse gas emissions can be greatly reduced.

Supplying the platforms with hydro power from the onshore power grid has long been discussed as a possible solution to the large emissions from the oil and gas industry. Economical aspects and potential reduction in greenhouse gases due to electrification from shore is investigated in [3]. Norwegian authorities have since 2007 required that power from shore must be considered for all new installations and major modifications on the continental shelf. Today the Troll A platform, and the fields Ormen Lange, Snøhvit, Gjøa, Valhall, and Goliat uses power from shore [6].

The potential for offshore wind power along the Norwegian cost is huge. In [7] it was estimated to 14 000 TWh, and it is claimed that the marked forces were the deciding factor on how much of this potential that were to be utilized. The main challenge with offshore wind power today is the large investments costs. The grid connection is considered a large cost and comprises roughly to 1/3 of the total costs. One way to reduce the costs is to operate the offshore wind farm together with one or more offshore oil and gas platforms in an isolated system. No systems like this are in operation today but several studies have been carried out investigating both economical aspects, possible fuel savings and emission reduction, as well as power system stability in such systems [8] [9]. The problem with this

configuration is that that since platforms need to operate also if there is no wind they still need a full scale power supply on board.

In a system containing offshore wind power and oil and gas platforms with a common connection to the onshore grid there will be little or no use for power generation on the platforms, and it also allows transfer of surplus power from the wind farm to the onshore power grid. Compared to building two separate grid connections this solution will not only lead to reduced investment cost, but also reduced transmission losses since the power from the wind farm can be utilized offshore. Due to the large consequences associated with black outs on oil and gas platforms it is essential that the wind farm don't obstruct the operations on the platforms. Offshore wind power is still a relatively new and immature technology and more research needs to be done to address the possibilities and challenges in systems containing offshore wind power.

This thesis will address stability issues in a system consisting of an offshore wind farm and several oil and gas platforms with a common High Voltage Direct Current (HVDC) connection to the onshore power grid based on Voltage Source Converter (VSC) technology. Similar systems with slightly different system configuration have been studied in [10] and [11]. It is important to review different system configuration regarding both technical and economical aspects.

1.2 Methodology and objective

The main goal of this project is to gain understanding of the system dynamics and the control of VSC-HVDC transmission system, offshore wind power, as well as offshore power systems. A hypothetical power system in the North Sea will be examined. The system is illustrated in Fig. 1.1 and consists of five oil and gas platforms and one offshore wind farm connected to the onshore power grid through a VSC-HVDC transmissions system. A dominant part of the work will be to create a dynamic simulation model of the system, a control strategy and a VSC-HVDC control system. Simulations of different system disturbances which are thought to be critical for the system operation will be made, to study the dynamics of the system and herby evaluate the feasibility of this system configuration. The simulation cases will represent large and partly exaggerated disturbances compared to what might be realistic, in order to test the limitations of the system. The system will be evaluated on whether it is able to stabilize after the disturbances and whether the voltage and frequency variations keep within the limits of the offshore grid code [12].

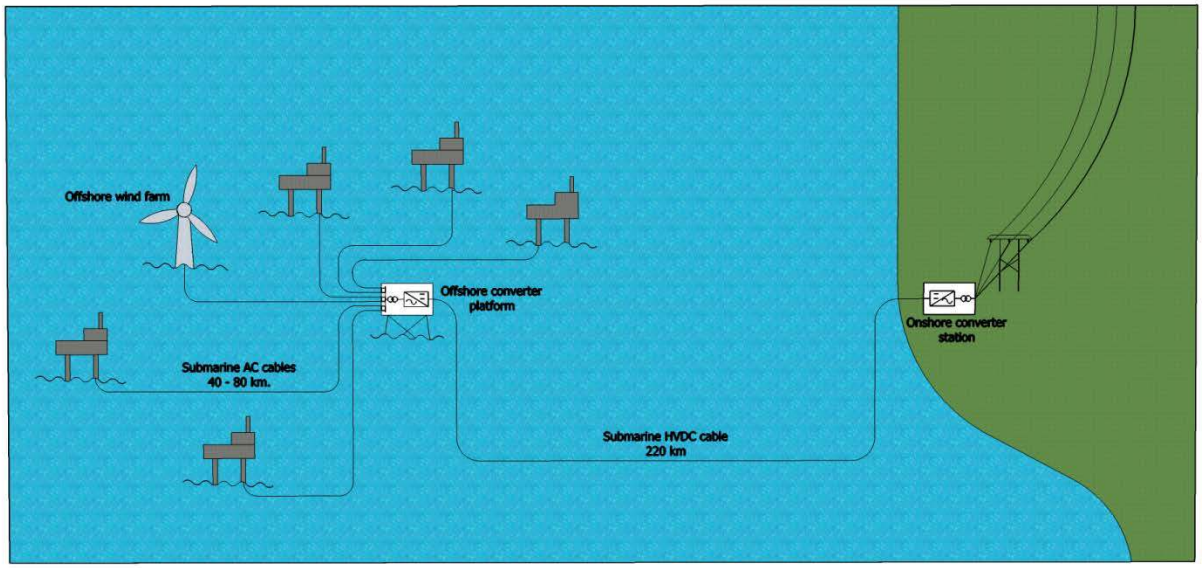

Fig. 1.1 Overview of the system.

2 VSC-HVDC

For long distance submarine power transmission VSC-HVDC are proving to be a very promising technology for several reasons [13]. Voltage source converters normally use Insulated Gate Bipolar Transistor (IGBT) unlike the more conventional Line Commutated Converters (LCC) [14] which uses thyristors. Because the IGBTs do not rely on the outer circuit for their commutation, VSCs, also known as self-commutated converters, are able to perform black starts. In contrast to the CSC the DC voltage of the VSC converter remains constant and the power flow is determined by the direction of the DC current. This enables the use of Cross-linked polyethylene (XLPE) cables, which are unable to deal with the polarity change in a CSC system. XLPE cables are less costly, lighter, and smaller in diameter than mass impregnated cables.

A schematic drawing of a two level, three-phase VSC is illustrated in Fig. 2.1. The voltages at the AC connections are a square wave switching between V_{DC} and $-V_{DC}$ depending on which switch is on. By using a switching frequency significantly higher than the fundamental frequency of the ac system a good approximation to a sine wave can be constructed. The amplitude, phase angle, and frequency of the AC side voltage are usually controlled based on pulse width modulation (PWM).

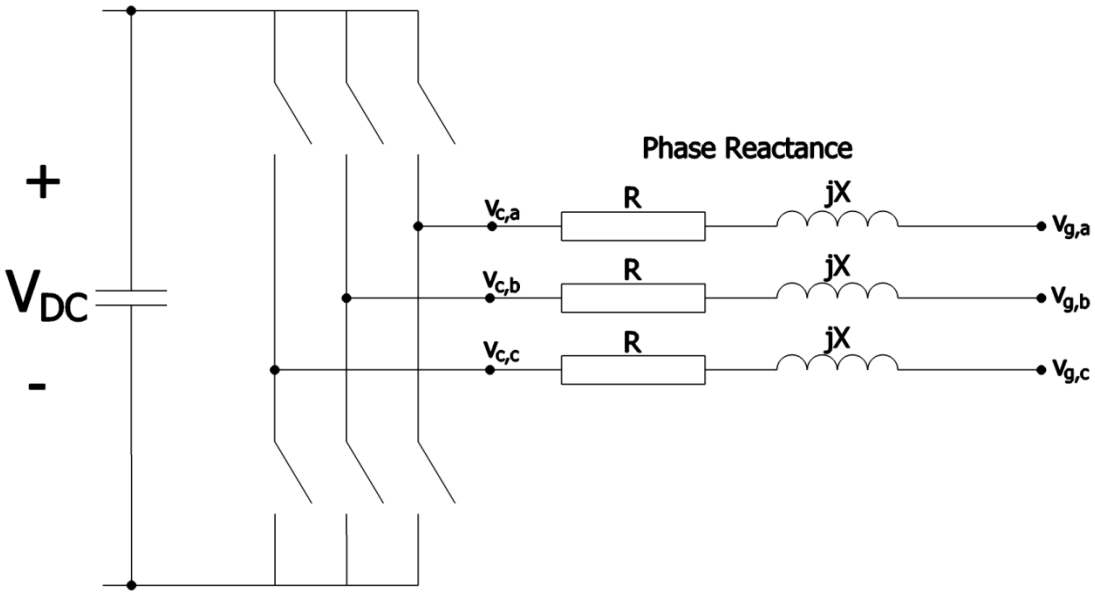

Fig. 2.1 Schematic drawing of a two level, three-phase Voltage Source Converter.

The phase-to-phase AC voltage will not be a perfect sinusoidal voltage but contains harmonics. These harmonics will be centered around multiples of the switching frequency. By using a high switching frequency the harmonics will occur at higher frequencies. This makes it easier to keep the total harmonic distortion at the connection point at a low level, compared to for a CSC.

In 2010 Siemens introduced a multilevel VSC technology called HVDC Plus and at the same time ABB upgraded their HVDC Light system to utilize a similar technology. In resent years several other companies also have introduced multilevel converters. The principle of the multilevel approach is illustrated in Fig. 2.2. A multilevel VSC builds up the AC voltage in small steps by using several sub modules consisting of

IGBTs and a DC link capacitor holding a part of the DC link voltage. In this way the switching frequency of each semiconductor can be reduced, hence reducing the switching losses in the converter. By using more steps the total harmonic distortion is also reduced, allowing the filters to be reduced or eliminated altogether [15].

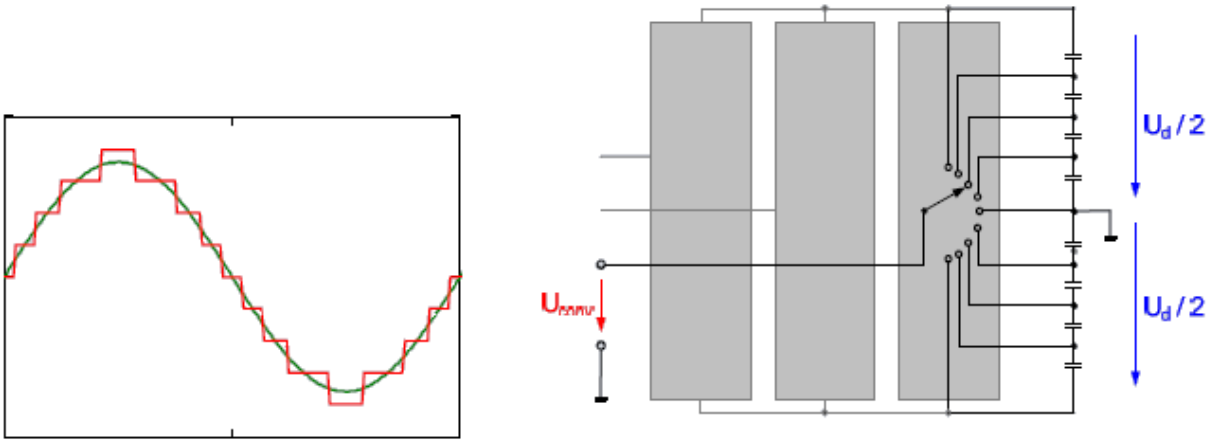

Fig. 2.2 Multilevel approach [15].

2.1 Operation of VSC

In both a pulse width modulated VSC and a multilevel VSC the converter voltage magnitude, frequency, and phase angle can be controller individually by the VSC controller. The operation of the VSC can be explained considering the schematic drawing in Fig. 2.1. The resistance of the phase reactance is normally so small compared to the reactance so it can be neglected. The active and reactive power into the ac side of the converter can then be described as in (2.1) referred to Vg.

$$P = \frac{V_g V_c \sin\delta}{X}$$
$$Q = \frac{V_g (V_g - V_c \cos\delta)}{X} \qquad (2.1)$$

It can be seen that δ, the angle between Vg and Vc, have a large effect on the active power while the converter voltage magnitude has a large effect on the reactive power. By controlling the phase angle and the amplitude of the converter voltage the converter can be operated in all four quadrants.

3 Modeling

An overview of the system can be seen in Fig. 3.1. If a system like this is to be realized it can not be built at the expense of the stability of the onshore power grid. The onshore connection is therefore thought to be at a strong point in the Norwegian main power grid. The grid connection is modeled as a Thevenin equivalent with phase-to-phase rms voltage equal to 300 kV, the frequency is 50 Hz, and the short-circuit level is set to 2500MVA. The transformers are modeled using a model referred to as the exact equivalent circuit in [16] and typical values are used. From the onshore converter the energy is transmitted through a 220 km HVDC bipolar transmission link. The offshore converter station and the AC busbar are thought placed on an offshore platform. Five oil and gas platforms with different load and one offshore wind farm are connected to the AC busbar. The distance from the converter platform to the oil and gas platforms and the wind park vary between 50 km – 80 km.

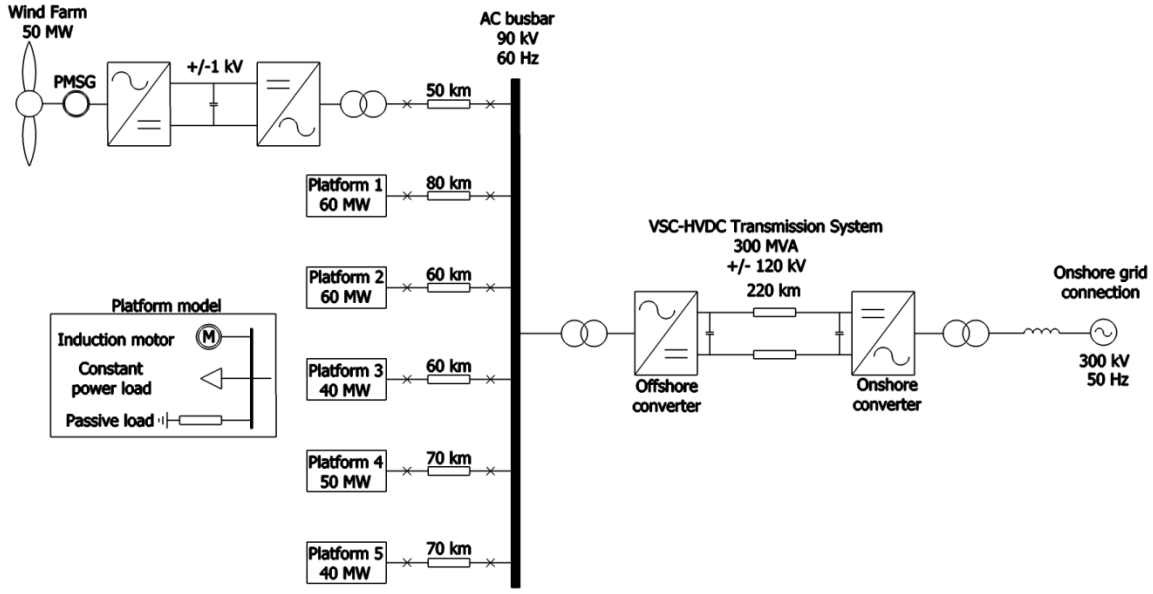

Fig. 3.1 Overview of the system.

3.1 Power transmission cables

All cables are modeled as a PI equivalent as illustrated in Fig. 3.2. Due to the long distance of the HVDC cable two PI sections are used in cascade. The voltage on the DC cable is +/- 120 kV and typical values are used. The offshore AC cables are modeled using one PI section, the voltage is set to 90 kV, and the parameters are taken from [17].

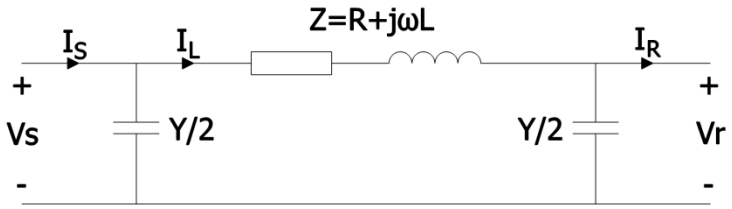

Fig. 3.2 Equivalent pi model for submarine cables.

The reactive power generated by the submarine cable can be expressed as the reactive power generated by the capacitances minus the reactive power consumed by the inductance as is (3.1).

$$Q_{Cable} = \frac{2}{Y}Vs^2 + \frac{2}{Y}Vr^2 - I_L{}^2\omega L \tag{3.1}$$

It can be seen that the reactive power generated by the cable is highly dependent of the voltage. In submarine power cables the capacitive elements normally dominate, causing the cable to generate reactive power under normal conditions.

3.2 Voltage source converter

This rapport aims to examine how the HVDC transmission system, the wind farm, and the oil and gas platforms interact, and how the control of the HVDC transmission influences the system dynamics. Converter losses and harmonic filters are not a focus point in this study. By utilizing a PWM modulated VSC with sufficiently high switching frequency or a multilevel VSC with a high number of steps the output approaches a pure sinusoid and harmonics can be neglected. This means that the converter can be modeled like a controlled voltage source generating the average AC voltage over one cycle of the switching frequency. This type of model is often referred to as an average model. It does not represent harmonics, but the dynamics cased by the controllers and the power system interaction is preserved. The average model can be used with larger time steps compared to a model including switches; hence the simulation time is reduced. Fig. 3.3 shows the VSC model used in this study. It is an ideal model so the active power on the AC side is always equal to the active power on the DC side as described in (3.2).

$$V_{conv,a} \cdot i_a + V_{conv,b} \cdot i_b + V_{conv,c} \cdot i_c = V_{DC} I_{conv} \tag{3.2}$$

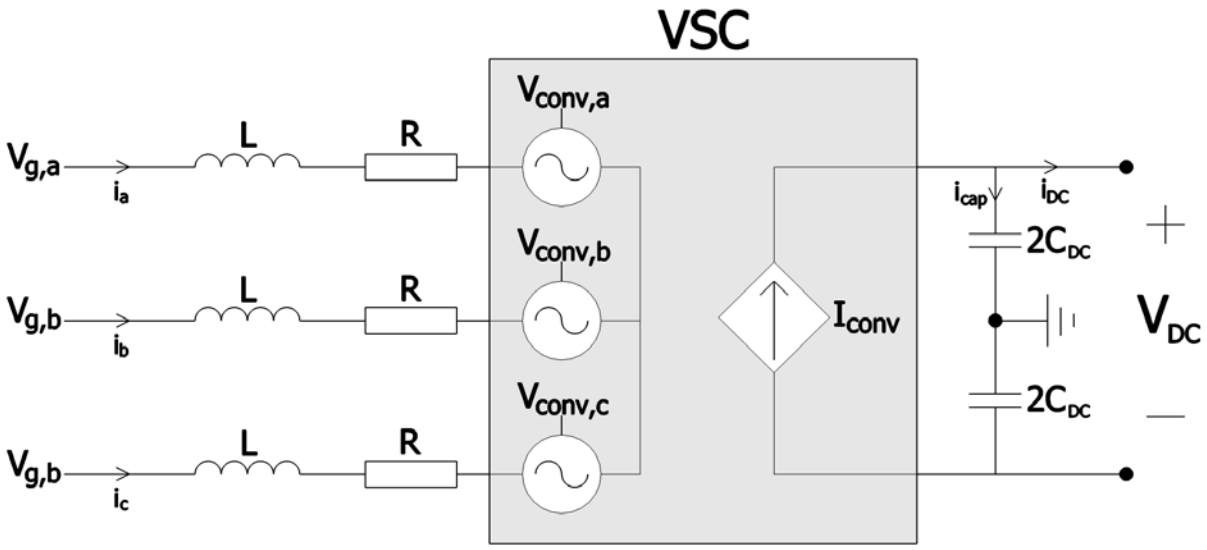

Fig. 3.3 Bipolar average model.

3.3 Wind farm

The wind farm model consists of a wind turbine, a Permanent Magnet Synchronous Generator, and a back to back VSC. A model of one wind turbine is made as illustrated in Fig. 3.4.

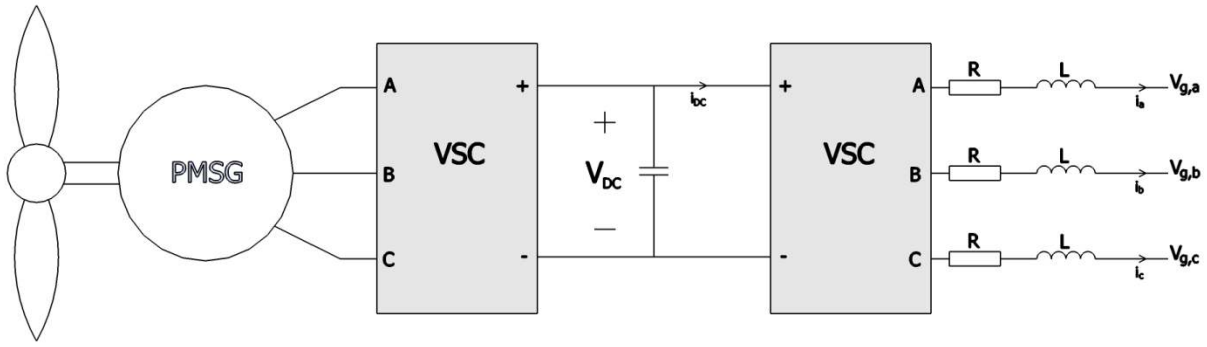

Fig. 3.4 Wind turbine model.

To reduce the simulation time an aggregated model, shown in Fig. 3.5, is used. The voltage at the wind farms connection to the grid is measured and used as input in a controlled voltage source supplying the wind turbine model. The current from the turbine model is measured and multiplied with the desired number of turbines in the wind farm before it is used as input in a controlled current source injecting current in to the grid. This model will behave as a wind farm consisting of “n” similar wind turbines all operating under the same wind conditions. The aggregation model also works as an ideal transformer with voltage ratio “k”, to represent the step-up transformer in the wind farm. In reality the wind speed will not be equal on all turbines in the wind farm at the same time but the total output power of the wind farm can be considered constant over a short period of time. Since this project only will consider the effect the wind farm has on the offshore system and not the interaction between each wind turbine,

or potential events that might occur in the collection grid of the wind farm, this is considered a valid simplification.

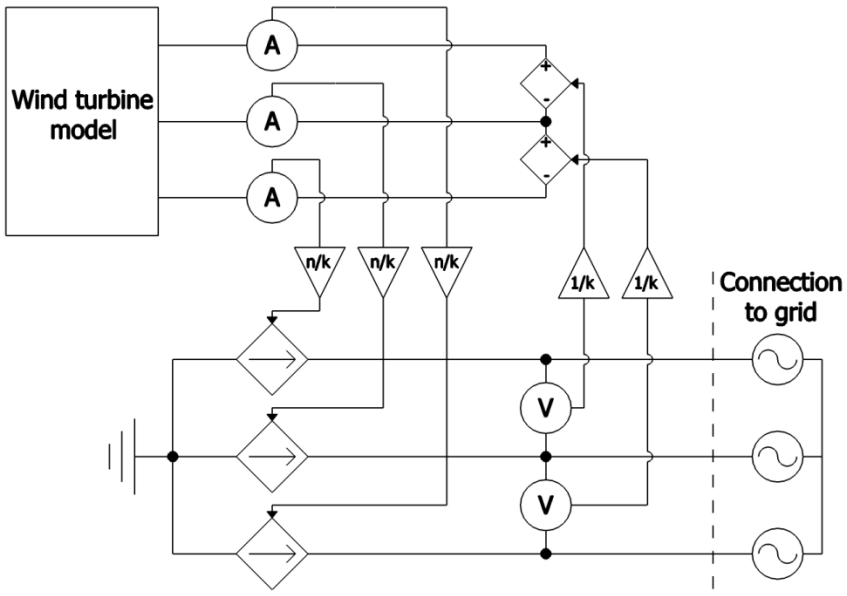

Fig. 3.5 Aggregated wind farm model

The parameters used in the wind farm model can be seen in Table 1.

Table 1 Wind farm data

Wind farm	
Number of turbines	25
Turbine	
Nominal output power	2 MW
Nominal wind speed	12 m/s
PMSG	
Nominal $V_{l\text{-}l}$	1 kV
Nominal power	2 MW
Number of poles	40
Inertia (rotor plus turbine)	8000 kg*m^2
DC link	
Nominal voltage	+/- 2 kV

3.3.1 Wind turbine

The wind turbine converts the kinetic energy from the wind into mechanical energy. To represent the wind turbine a model found in the SimPowerSystems library in MATLAB®/Simulink® is used. The output power of the turbine, P_m, is given in (3.3).

$$P_m = C_p(\lambda, \beta)\frac{\rho A}{2}v_{wind}^3 \quad \textbf{(3.3)}$$

C_p is the performance coefficient of the turbine, ρ is the air density, A is the rotor area, and v_{wind} is the wind speed. C_p is given in (3.4) [18],

$$C_p(\lambda,\beta) = 0.5175 \cdot (\frac{116}{\lambda_i} - 0.4\beta - 5) \cdot e^{\frac{-21}{\lambda_i}} + 0.0068 \cdot \lambda$$

$$\frac{1}{\lambda_i} = \frac{1}{\lambda + 0.08\beta} - \frac{0.035}{\beta^3 + 1} \qquad \textbf{(3.4)}$$

where β is the pitch angle of the rotor blades in degrease and λ is the ratio of the rotor tip speed to wind speed.

From (3.3) it can be shown that the power from the wind turbine is proportional to C_p. Fig. 3.6 illustrates C_p as a function of the tip speed ratio λ for different values of pitch angle β. C_{pmax}=0.4667 is found for β=0° and λ=8.1. This value for λ is called λ_{nom} and is used in the control of the wind turbine as this is the tip speed ratio that gives the highest output power for any wind speed as long as β=0°. The pitch angle is used to limit the output power when the wind speed exceeds nominal speed.

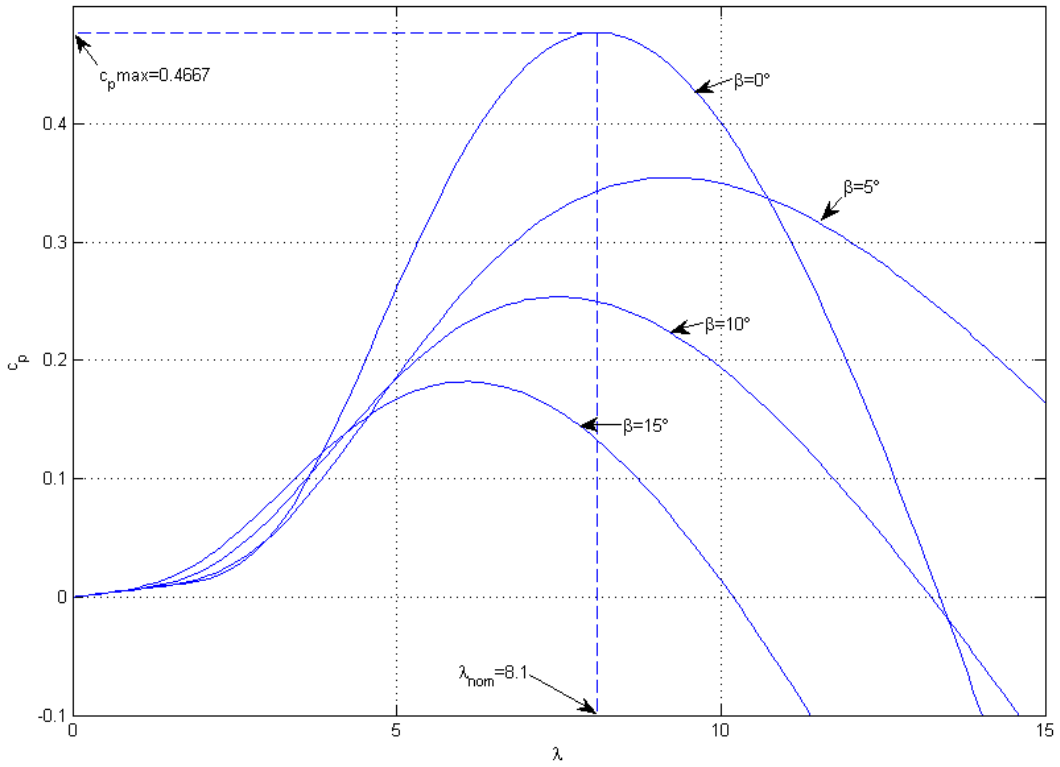

Fig. 3.6 C_p – λ characteristics for different values of pitch angle β.

The mechanical output power as a function of turbine speed for different wind speeds and pitch angle β=0 is illustrated in Fig. 3.7. It can be noticed that for every wind speed there is an optimal turbine speed

that produces the maximum amount of power. By setting $\lambda=\lambda_{opt}$ the optimal turbine speed is proportional to the wind speed as shown in (3.5).

$$\omega_{ref} = \frac{\lambda_{opt} v_{wind}}{r_{blades}} \tag{3.5}$$

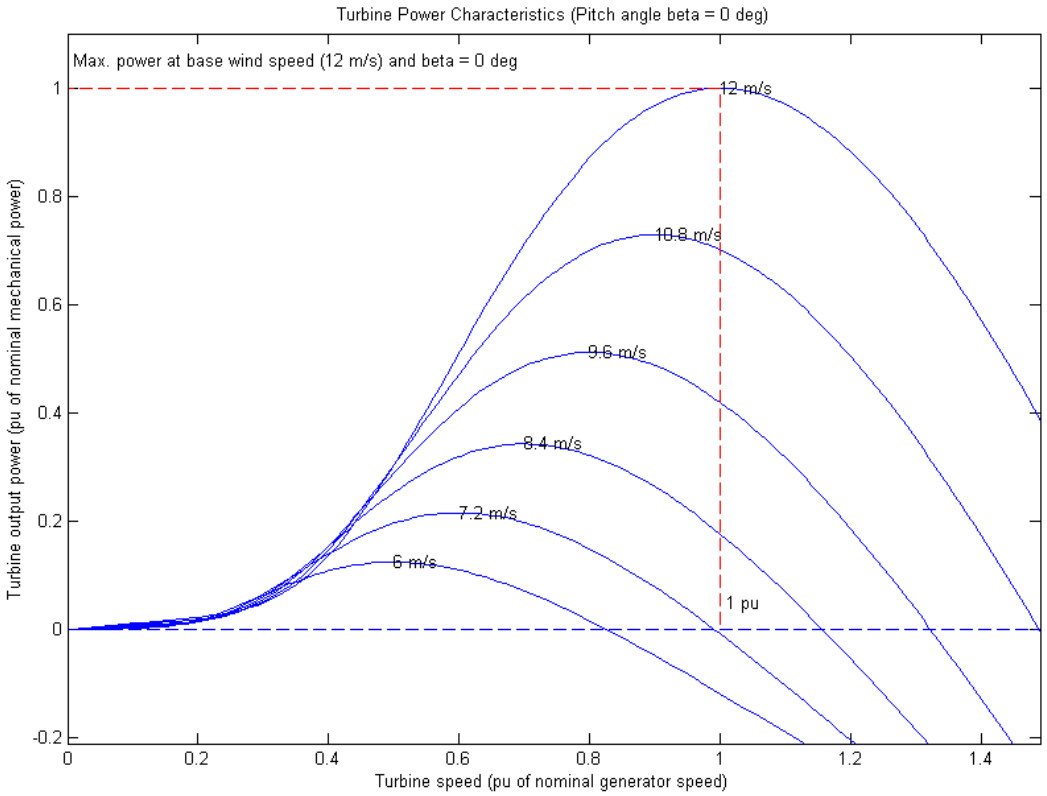

Fig. 3.7 Output power of the wind turbine as a function of turbines speed for different wind speeds [19].

3.3.2 Permanent Magnet Synchronous Generator

To represent the PMSG a three phase sinusoidal model from the SimPowerSystems library in MATLAB®/Simulink® is used. This model is based on the equations (3.6) and (3.7) [19]. The equations are based on a dq reference frame where the d-axis is aligned with the rotor flux. All quantities are referred to the stator.

$$\begin{aligned} \frac{d}{dt} i_d &= \frac{1}{L_d} v_d - \frac{R}{L_d} i_d + \frac{L_q}{L_d} p\omega_r i_q \\ \frac{d}{dt} i_q &= \frac{1}{L_q} v_q - \frac{R}{L_q} i_q - \frac{L_d}{L_q} p\omega_r i_d - \frac{\lambda p\omega_r}{L_q} \end{aligned} \tag{3.6}$$

$$T_e = 1.5\, p[\lambda i_q + (L_d - L_q) i_d i_q] \tag{3.7}$$

$v_{d,q}$ and $i_{d,q}$ are the d- and q-axis voltage and currents. $L_{d,q}$ is the d- and q-axis inductance, R is the resistance in the stator windings, ω_r is the angular rotation of the rotor, λ is the amplitude of the flux induced by the permanent magnets in the rotor in the stator phases, p is the number of poles, and T_m is the electromagnetic torque. In this study a round rotor machine is used. That means that the d- and q-axis inductances are equal, so:

$$L_d = L_q = \frac{L_{ab}}{2} \tag{3.8}$$

Inserting (3.8) into (3.7) gives:

$$T_e = 1.5 p \lambda i_q \tag{3.9}$$

The mechanical system of the model is based on (3.10).

$$\frac{d}{dt}\omega_r = \frac{1}{J}(T_e - F\omega_r - T_m) \qquad \frac{d\theta}{dt} = \omega_r \tag{3.10}$$

J is the combined inertia of the rotor and the load, F is the combined viscous friction of the rotor and the load, θ is the rotor angular position, and T_m is the mechanical torque on the shaft.

3.4 Oil and gas platform

The load on an oil and gas platform can roughly be divided in to three types of load: direct online AC motors, variable speed drives, and passive loads [20]. The total electric power demand, and distribution between the different types of load, can vary greatly depending on the design of the platform and the operations running on the platform.

The load on the platform models used in this project is determined in cooperation with representatives from Statoil and given in Table 2.

Table 2 Load distribution on oil and gas platforms.

Passive load	50 %
VSD	40 %
Direct online AC motors	10 %

To study the influence on the platform load, alternative load distributions will also be simulated.

3.4.1 Asynchronous motor

Direct on line AC motors operating at constant speed are used for water injection pumps, pumps for cooling water or other cooling medium, air and gas compressors and ventilation fans. To model these motors an asynchronous motor model is taken from the SimPowerSystems library in

MATLAB®/Simulink®. The electrical part of the model is represented by a fourth-order state-space model based on a dq reference frame. The induced electromagnetic torque of the motor is given in (3.11),

$$T_e = 1.5p(\lambda_{ds} i_{qs} - \lambda_{qs} i_{ds}) \quad \textbf{(3.11)}$$

where p are the number of pole pairs, $\lambda_{d,q\,s}$ is the d- and q-axis stator flux, and $i_{d,q\,s}$ is the d- and q-axis stator current. In [21] it is shown that the torque of an induction motor is proportional to the square of the stator voltage. The voltage on the platform will therefore be of great importance to the torque induced in the motor.

The speed of the induction motor is given in (3.12) where J is the combined inertia of the rotor and the load.

$$\frac{d}{dt}\omega_m = \frac{1}{2J}(T_e - F\omega_m - T_m) \quad \textbf{(3.12)}$$

The mechanical load, Tm, of the motor is set to vary with the rotational speed, ω_m, as stated in (3.13). This is typical for pumps and fans.

$$T_m = 0.2 + 0.8\omega_m^2 \quad \textbf{(3.13)}$$

The torque-speed characteristic during acceleration for the motor and the load curve are plotted in Fig. 3.8. Immediately after applying the stator voltage the instantaneous torque varies at line frequency around an average positive value. This decaying 60 Hz oscillation is due to the interaction between the rotating flux and the dampened DC flux that appear when current starts to flow in the machine [22]. It can also be noticed that the speed overshoots the rated speed and the instantaneous torque and the speed oscillates before the speed stabilizes. This is typical for large horsepower machines [21].

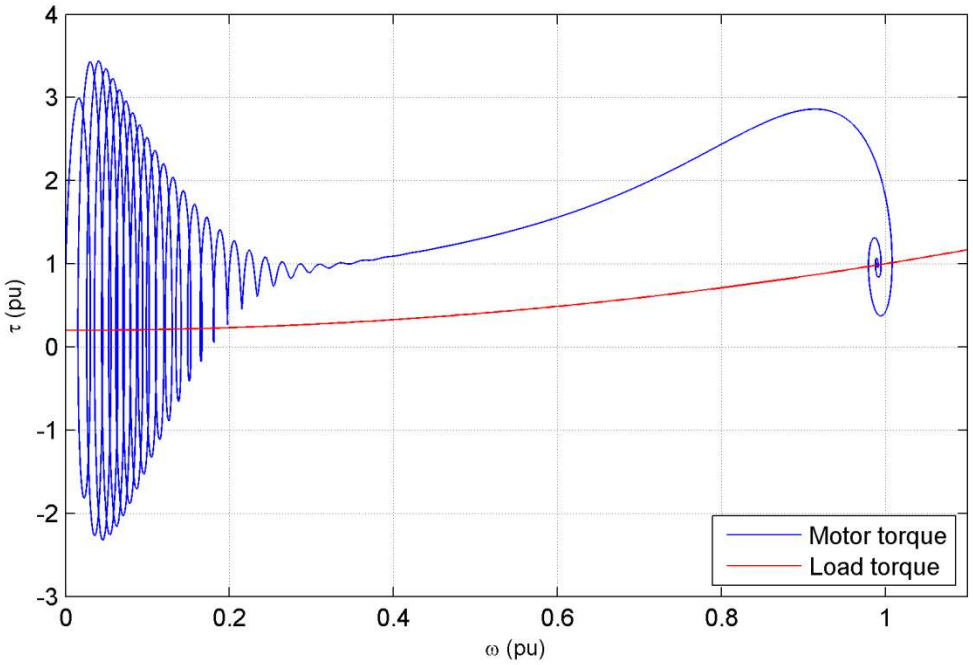

Fig. 3.8 Induced torque in the motor and the load torque versus rotational speed during acceleration of the motor.

To reduce simulation time and complexity of the model an aggregated model is used. In reality the motors will be of different size and hereby have different inertia. They will also carry different mechanical loads. To create a model of all different motors on the platforms would be a very challenging and time consuming task. The motor parameters and the motor load will influence the dynamics of the system and has to be taken into account when analyzing the simulation results.

3.4.2 Variable speed drives

Variable speed drive AC motors is used for big motors that cannot be started direct online and for equipment that require variable speed like main drilling motors, pumps, and fans.

In order to control the speed of an ac motor a switch-mode dc-to-ac inverter are used. The objective of this inverter is to control the magnitude and the frequency of the motor voltage to achieve the desired speed and torque on the motor. The dc voltage is obtained by ether a diode rectifier, or for applications where regenerative breaking is required, a switch-mode rectifier. If a diode rectifier is used, the dc link voltage will vary with the grid voltage. The inverter should then react quick enough to these changes is the dc voltage and keep the motor voltage and frequency at the defined level. The motor will then be unaffected by small changes in the grid voltage and the power consumed by the motor, thus the active power drawn from the grid will remain constant.

If a switch-mode rectifier is used it will try to keep the voltage on the dc link constant. The inverter and the motor will therefore be unaffected by changes in the grid voltage and the power consumed by the drive remains constant.

To model variable speed drives on the oil and gas platforms a constant power load is used. The main reason for this is to reduce the simulation time. Fig. 3.9 shows one phase of the model. The model measures the voltage over a controlled current source and then calculates the current needed to achieve the wanted active power. This signal is then used as input in the controlled current source.

This model will set up the current needed to achieve the desired power regardless of the system voltage. In the converter current limits will restrict the maximum power if the voltage gets to low. But since this thesis only study load variations causing relatively small variations in the grid voltage this, is considered a valid simplification.

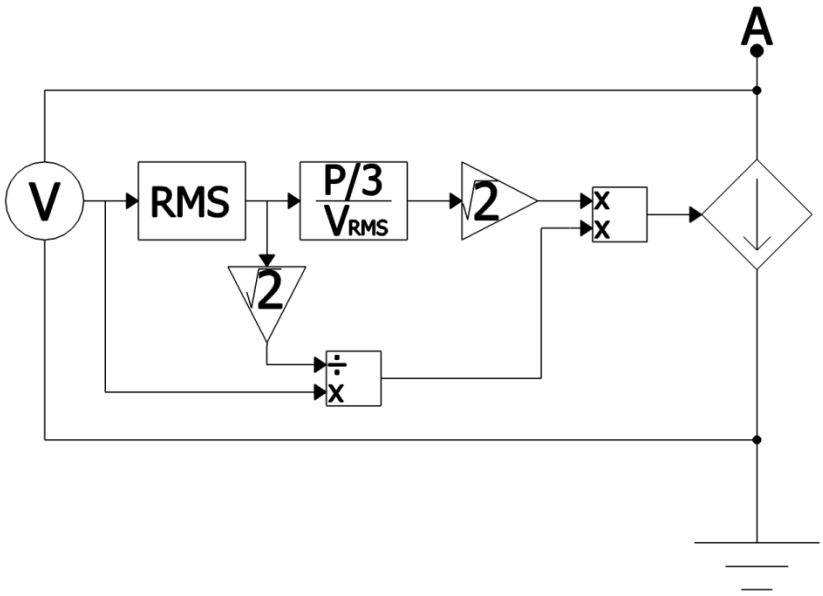

Fig. 3.9 Constant power load.

3.4.3 Passive loads

Oil and gas platforms also have a vast demand for electric power for gas drying equipment, boilers, lights, and heating of multiphase pipelines to avoid hydrations. The larges part of the passive loads is believed to be heaters so the passive load is modeled purely resistive.

4 Control system

The main goal of the control system is to let the wind farm produce maximum amount of active power at all times and let the VSC-HVDC transmission system assure that the oil and gas platforms have stable operating conditions with as little voltage and frequency fluctuations as possible. This is realized by the following control objectives:

- The wind turbine generator side converter controlling the speed of the turbine.
- The wind farm grid side converter controlling the DC link voltage.
- The offshore VSC-HVDC converter controlling the frequency and the voltage on the offshore busbar.
- The onshore VSC-HVDC converter assuring stable operating conditions for the offshore converter by controlling the estimated voltage offshore DC-terminals.

4.1 Control principle

The control of the VSCs is achieved using vector control based on a synchronous rotating dq- reference frame. All three-phase voltages and currents are represented as vectors in a stationary α-β coordinate system, where the α-axis is oriented along the a-axis in the three-phase system and the β-axis is 90° ahead of the α-axis. A rotating d-q reference frame, synchronized with the AC grid, is then introduced. See Fig. 4.1. Since the d-q frame is synchronized with the grid it rotates at a speed of ω with respect to the α-β reference frame. All voltage and current vectors will therefor occur as constant vectors in the d-q frame. Any static errors can therefor be avoided using PI controllers.

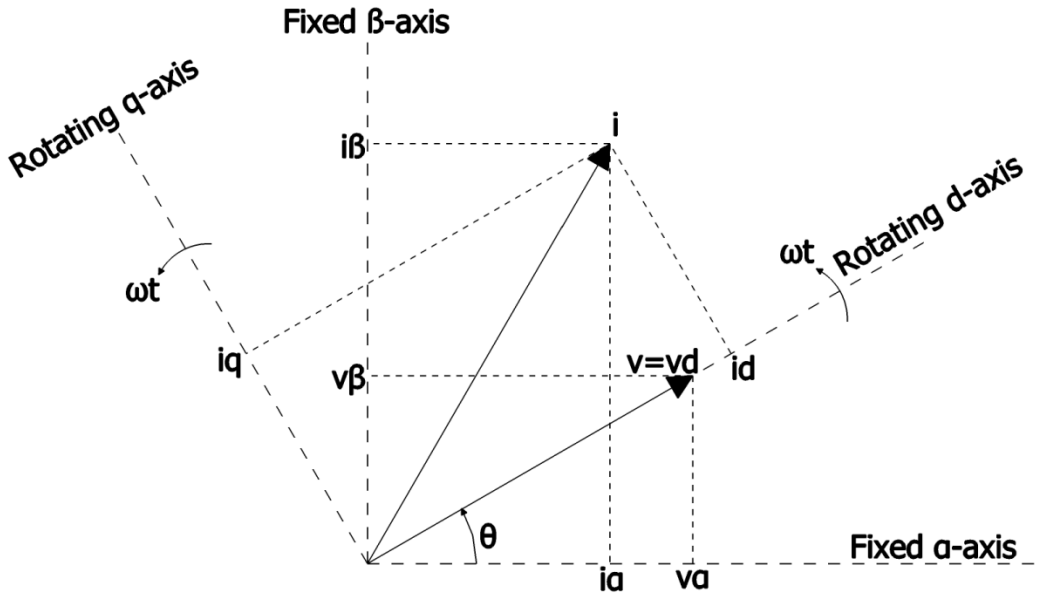

Fig. 4.1 Transformation of α-β and d-q axis.

The angle between the α-β and the d-q reference frame is given by θ=ωt. This is computed using a phase lock loop (PLL).

Using the d-q transformation the voltages of the converter can be described as:

$$v_{g,d} - v_{d,conv} = Ri_d + L\frac{di_d}{dt} - \omega Li_q$$
$$v_{g,q} - v_{q,conv} = Ri_q + L\frac{di_q}{dt} + \omega Li_d \quad (4.1)$$

where $v_{g,dq}$, $v_{conv,dq}$, and i_{dq} are the d and q part of the AC grid voltage, the converter terminal voltage, and the line current respectively [23]. R and L are the resistance and the inductance between the converter and the AC grid connection point.

The control circuits in this project are built up using per unit quantities. Calculations of base values are found in appendix A. A cascaded control system is used consisting of a fast inner current controller and a slower outer controller, controlling the active power or DC voltage, and reactive power, or AC voltage.

4.2 Inner current controller

The inner current controller is similar for the wind farm control system and the VSC-HVDC onshore control system and is illustrated in Fig. 4.3, Fig. 4.7 and Fig. 4.9. It uses a PI regulator to track the d- and q-axis AC current references. As seen in (4.1) there is a relation between the two axes. This is compensated for using feed-forward de-coupling terms. The resulting signal is carried through a dq to abc transformation and used as voltage references in the VSC average model.

The controller is tuned based on simulations in order to achieve a fast response. The response of the inner current controller is tested by connecting the VSC model to a fixed DC voltage source and applying a step change in id at t=0.3 s and iq at t=0.32 s. From Fig. 4.2 it can be seen that the settling time is around 2 ms. Id has a small impact on iq and vice versa. This impact would be greater without the feed-forward terms.

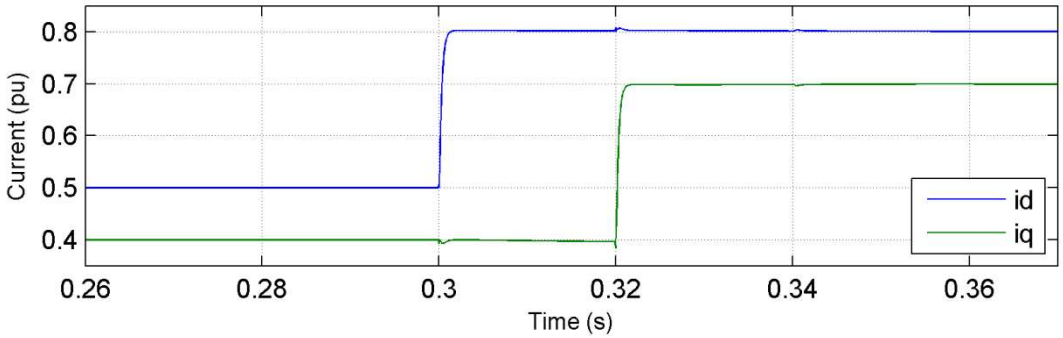

Fig. 4.2 Response of inner current controller.

4.3 Onshore converter

In the control system of the onshore converter the d-axis of the rotating reference frame is aligned to the AC grid voltage vector. The instantaneous active- and reactive power injected or absorbed from the AC system is therefore given by (4.2) [24].

$$P = \frac{3}{2} v_d \cdot i_d$$
$$Q = -\frac{3}{2} v_d \cdot i_q \quad \textbf{(4.2)}$$

It is possible to control active- and reactive power independently by controlling the d- and q- axis current. By controlling the active power injected in to the HVDC link, the DC voltage can be controlled, and by controlling reactive power the AC voltage can be controlled.

The onshore converter control system is shown in Fig. 4.3. The objective of the outer controller is to keep the DC voltage on terminals of the offshore converter at a fixed level. This is done by calculating the voltage drop in the DC cable and adding it to the voltage reference. The difference between this value and the measured DC voltage on the onshore terminals are then minimized by a PI controller. To minimize the slower response associated with a cascaded control system the reference value of the inner controller is fed-forward. In this way variations in the outer control loop are reduced hence the gain in the controller can be reduced, which is important for the stability [24]. From (3.2) and (4.2) it can be shown that under balanced conditions, i_{cap}= 0, the reference value for id should be $V_{DC,comp}$ stated in (4.3).

$$V_{DC,comp} = \frac{V_{DC,pu}}{v_{d,pu}} \cdot I_{DC,pu} \quad \textbf{(4.3)}$$

$V_{DC,pu}$ is the voltage on the DC cable, $I_{DC,pu}$ is the current in the DC cable and $v_{d,pu}$ is the d component of the AC voltage

The onshore controller can in in addition control the AC voltage or reactive power to the onshore grid and in this way help stabilizing the onshore power system. This is not a focus point if this study and since the onshore grid connection is considered a strong point in the main power grid this is not thought to be necessary and not treated further. $I_{q,ref}$ is set to zero.

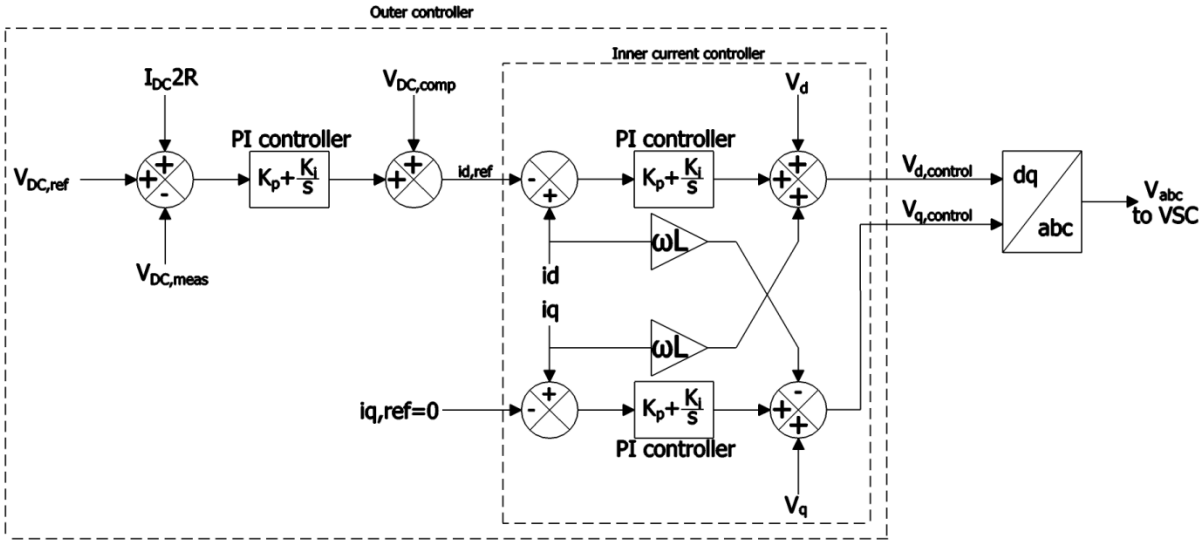

Fig. 4.3 Onshore converter control system.

The DC voltage controller is tuned based on simulations and the objective is to achieve a stable system with minimal voltage oscillations. The response of the converter was tested by disconnecting the offshore converter and letting the onshore converter control the voltage on the offshore termination of the DC cable. Fig. 4.4 shows the response of the DC voltage when a step change in the voltage reference is applied at t=0.4 s.

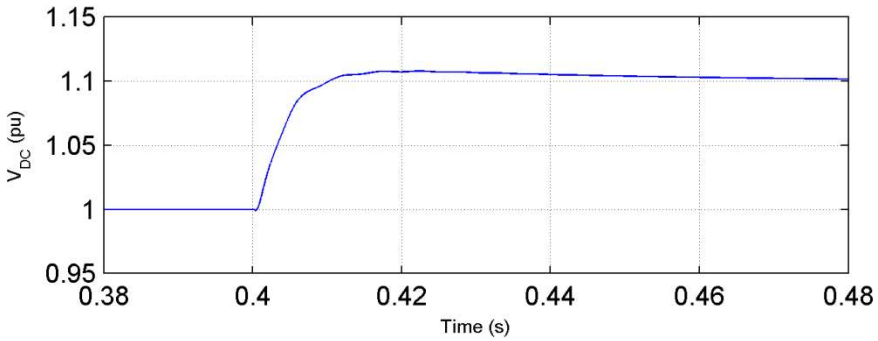

Fig. 4.4 Response of onshore converters DC controller.

4.4 Offshore converter

The offshore converter is responsible to keep the voltage on the AC busbar constant. The control system for the offshore converter is illustrated in Fig. 4.5. Unlike the other control circuits this controller does not use vector control. The difference between the measured voltage on the busbar and the voltage reference is minimized by a PI controller. The output is then multiplied with a fixed three phase, 60 Hz sinusoidal signal before it is used as a reference signal in the VSC model. In this way the frequency on the offshore AC system will remain constant at 60 Hz.

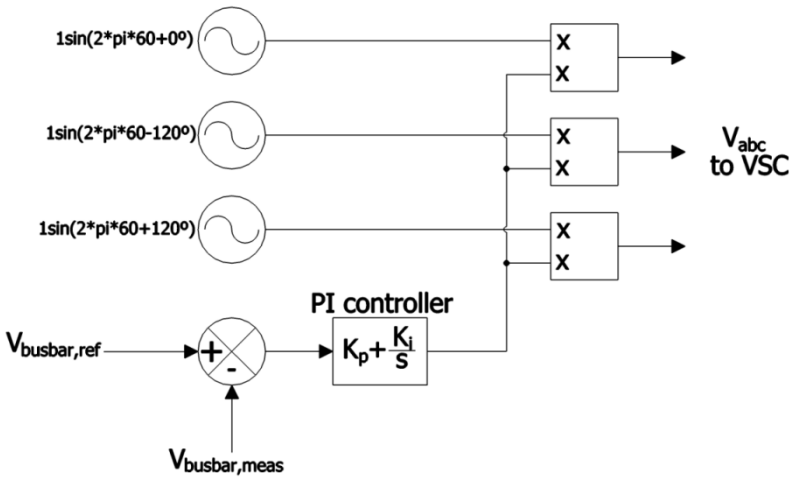

Fig. 4.5 Control system for the offshore converter.

The offshore voltage controller is tuned based on simulations to achieve a stable system with minimal voltage oscillations. The response of the controller is tested by applying a step in the voltage reference at t=1.5 s. The response is shown in Fig. 4.6.

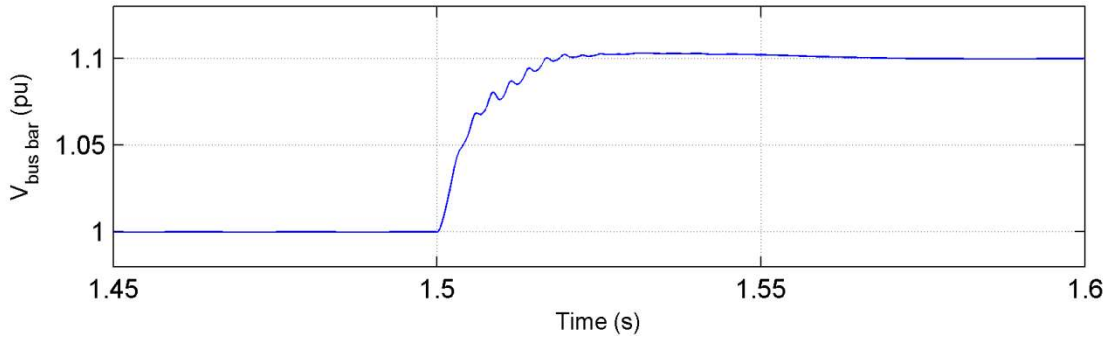

Fig. 4.6 Response of voltage controller on offshore converter.

4.5 Wind farm

The goal of the wind farm controller is to produce the maximum amount of active power for any given wind speed. This is realized by letting the generator side controller control the speed of the permanent magnet synchronous generator. The grid side controller will control the DC link voltage and the reactive power to the offshore AC grid.

4.5.1 Generator side controller

To extract the maximum amount of power from the wind the tip speed ratio λ should be as close to λ_{nom} as possible. The d-axis is aligned with the rotor flux. From (3.9) it can be seen that by controlling iq the electromagnetic torque can be controlled and hereby the speed of the generator according to (3.10). The outer controller takes the wind speed as input and calculates the speed reference for the PMSG using the correlation between wind speed and rotational speed of the turbine given in (3.5).

The difference between the speed reference and the measured speed is used as input in a PI controller where the output is used as reference for the q-axis current. The control system for the generator side converter in the wind farm is illustrated in Fig. 4.7.

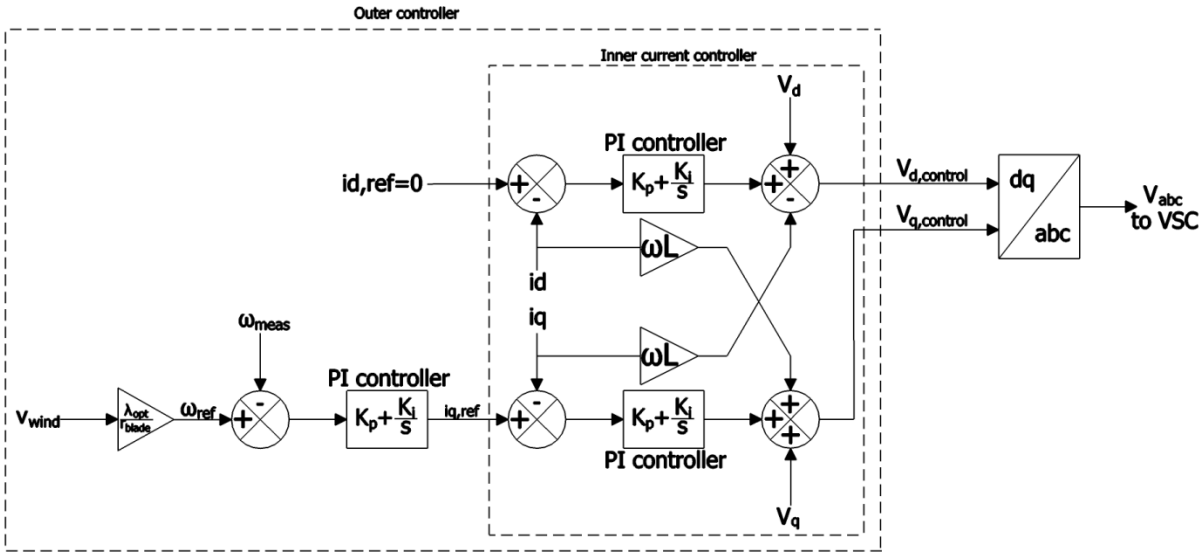

Fig. 4.7 Control system for the generator side converter in the wind farm.

A negative id current will cause flux weakening in the machine [25]. This can be utilized to keep the induced voltage in the generator from exceeding the rated voltage for generator speeds beyond rated speed. In this study the generator speed will be kept within the ratings so the d-axis current is kept to zero.

The converter is tuned based on simulations in order to get stable system with minimal oscillations. The response is tested by applying a step change in the speed reference at t=0.8 s. The response is shown in Fig. 4.8.

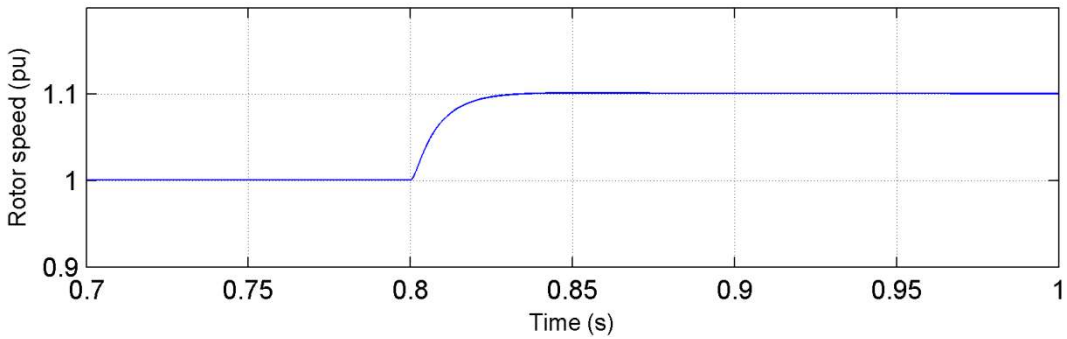

Fig. 4.8 Response of the speed controller on the wind side converter in the wind farm.

The inertia of the turbine is set relatively low to speed up the acceleration of the turbine.

4.5.2 Grid side controller

The control system for the grid side converter in the wind farm is shown in Fig. 4.9. The grid side converter is responsible for controlling the voltage on the DC link. This is done in the same way as for the onshore converter. See 4.3. The grid side controller also controls the reactive power into the busbar. In this project Q_{ref} is set to zero.

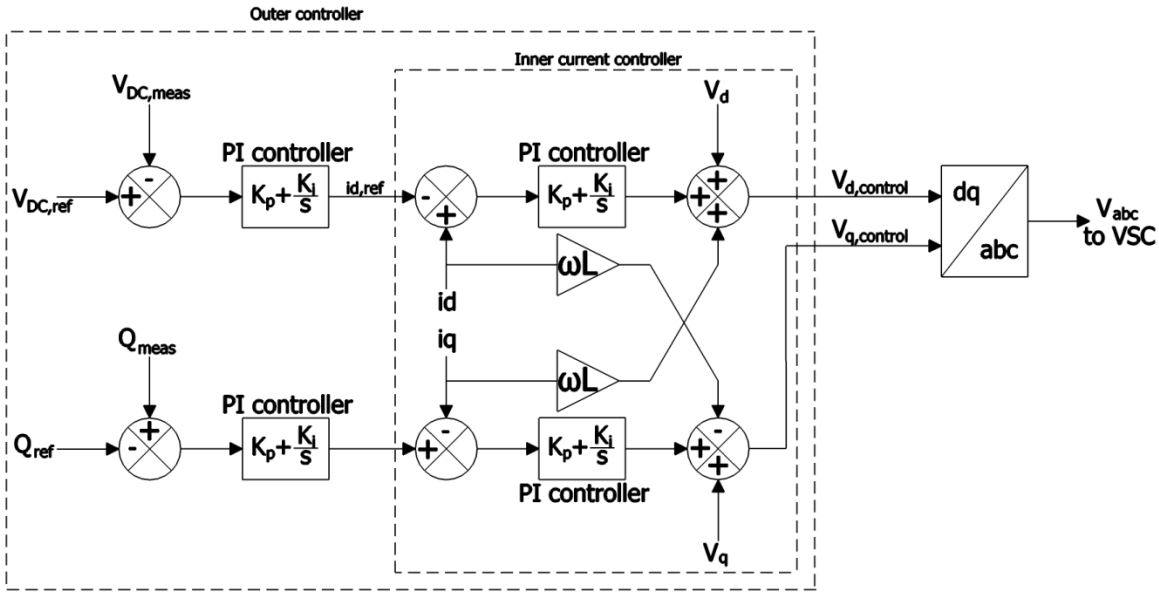

Fig. 4.9 Control system for the grid side converter in the wind farm.

Tuning of the controller has been performed based on simulations to achieve a stable system. The response of the controller was tested by applying a step change in the reference values. The response can be shown in Fig. 4.10.

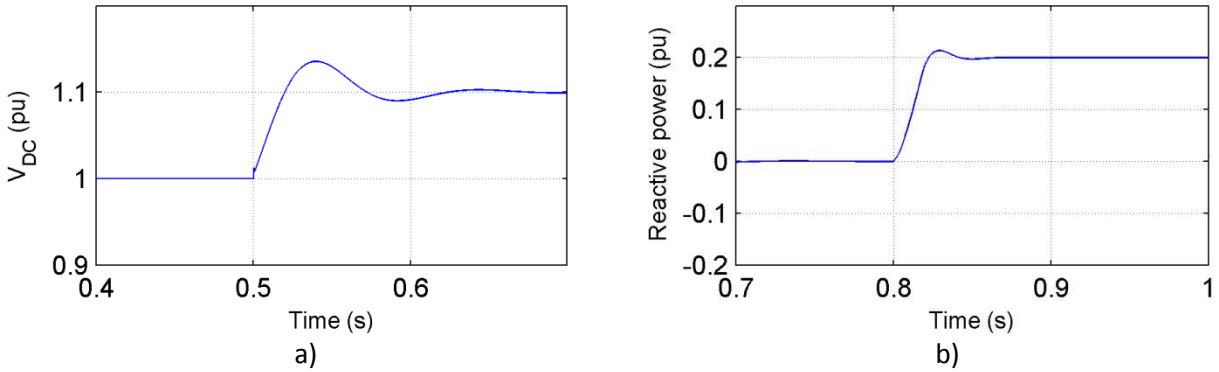

Fig. 4.10 a) Response of the DC voltage controller on the grid side converter in the wind farm. b) Response of the reactive power controller in the grid side converter in the wind farm.

4.5.3 Pitch angle controller

When the wind speed exceeds the rated speed of the turbine the torque on the rotor blades and hence the output power will exceed the ratings of the turbine and the PMSG. To limit the torque on the rotor blades the pitching of the blades are then changed with an angle β. The pitch controller is illustrated in Fig. 4.11. The error between the rated power and the measured power of the generator are minimized

by a PI controller. There is a limitation on how fast the rotor blades can turn, hence how fast the pitch angle can change. This is taken in to account with the rate limiter. The error between the measured wind speed and the wind speed reference is run through a P controller and used as feed forward for a faster response.

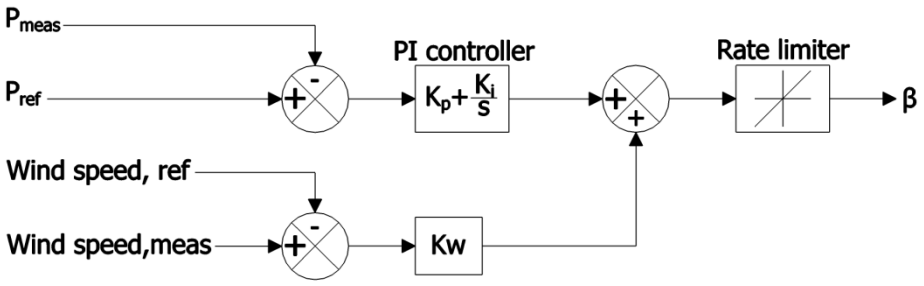

Fig. 4.11 Pitch controller.

In the simulations the wind speed is kept under nominal wind speed so the pitch controller is not active.

5 Simulation results

To investigate the sturdiness of the system, simulations are performed using the toolbox SimPowerSystems in MATLAB®/Simulink®. Different disturbances will be introduced and the power system will be evaluated on whether it is able to stabilize after these disturbances. The voltage and frequency variations will also be compared with the limits given in IEC 61892 which is the norm regarding offshore electric installations [12]. The allowed transient and static, voltage and frequency variations on oil and gas platforms are stated in Table 3.

Table 3 Important parameters given in IEC 61892.

Platform parameter	Limits in per unit
Transient voltage limits	0.8 – 1.2
Stationary voltage limits	0.9 – 1.06
Transient frequency limits	0.9 – 1.1
Stationary frequency limits	0.95 – 1.05

5.1 Lose wind power.

Short circuits, faults in cables, protection system, or other occurrences may lead to tripping of the wind farm. It is then important that the VSC-HVDC control system is able to handle this disturbance so that the effects on the platform are marginal. In the first simulation case the wind farm is set to deliver 50 MW before it is disconnected. The HVDC-VSC transmission system then has to react quickly to compensate for the lost power generation. The wind farm is disconnected at t=2 s and the results of the simulation are shown in Fig. 5.1 - Fig. 5.10.

The RMS voltage on the busbar, platform 1, and the DC voltage on the offshore terminals during disconnection of the wind farm are shown in Fig. 5.1. When the wind farm is disconnected the voltage on the busbar drops but the controller on the offshore converter reacts quickly to reestablish the voltage. The voltage on platform 1 is similar to the voltage on the busbar except the voltage drop in the AC cable. There is a negative peak in the platform voltage on approximately 0.6 pu and there are some minor oscillations before the voltage stabilizes after 0.01 s. The platforms voltage is well within the limits in Table 3 and since platform 1 has the largest load and the longest transmission cable the voltages on the other platforms can also be assumed to be within the limits.

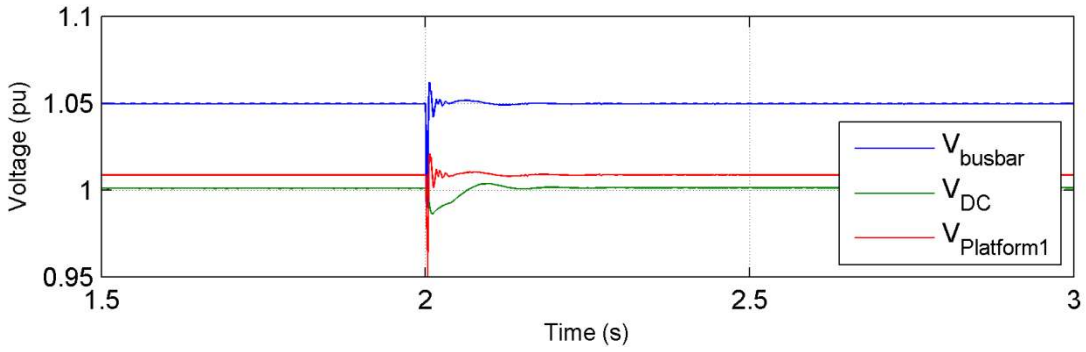

Fig. 5.1 Voltages in the system during disconnection of the wind farm.

The active power flow in the system is illustrated in Fig. 5.2. The power from the offshore converter is quickly increased to meet the demand of the platforms. It can also be seen that the power drawn from the onshore grid have larger oscillations than the power from the offshore converter due to the losses in the DC cable. The power on the offshore terminals on the DC cable is similar to the power from the offshore converter except the losses in filter and the transformer.

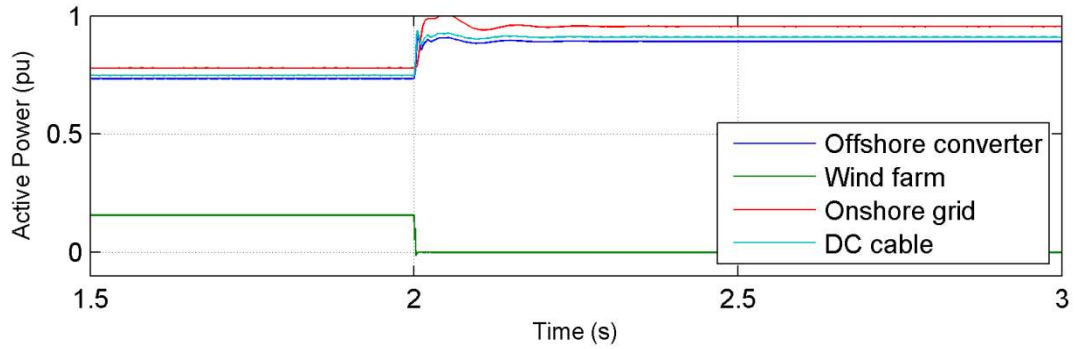

Fig. 5.2 Active power in the system during disconnection of the wind farm.

Fig. 5.3 shows the frequency on the offshore busbar during disconnection of the wind farm. The nature of the offshore controller should imply a fixed frequency on the busbar. The minor oscillations and deviation from the fundamental frequency are most likely an error in the measurement block. See chapter 6 for further discussion. The frequency is however well within the limits in Table 3.

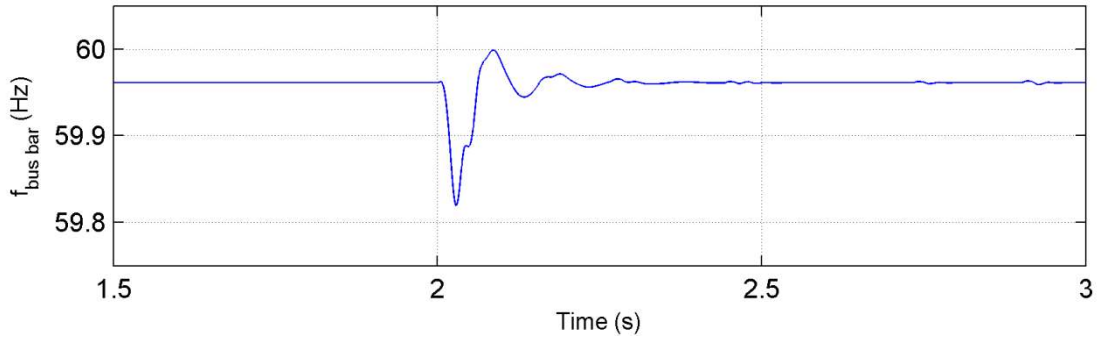

Fig. 5.3 Frequency on the busbar during disconnection of the wind farm.

Fig. 5.4 shows the distribution between the different loads on platform 1. As mentioned in 3.4.1 the torque in an induction motor is proportional to the motor terminal voltage squared. The small dip in the platform voltage will therefore cause a minor oscillation in the speed and thus in the power to the induction motor. This power oscillation can also be seen in the power drawn from the onshore power grid in Fig. 5.2.

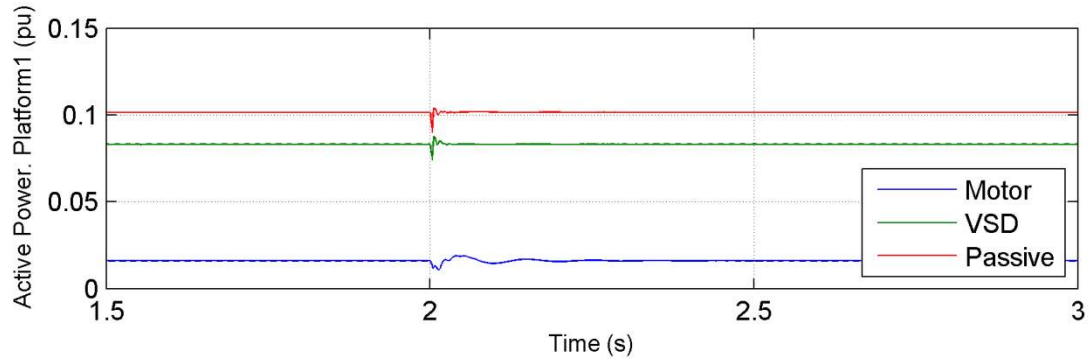

Fig. 5.4 Load distribution on platform 1.

Fig. 5.5 shows the voltage at the connection point to the onshore power grid. Due to the increased load the voltage drops. This could be prevented with the use of dynamic reactive power control on the onshore converter but this is not examined in this project.

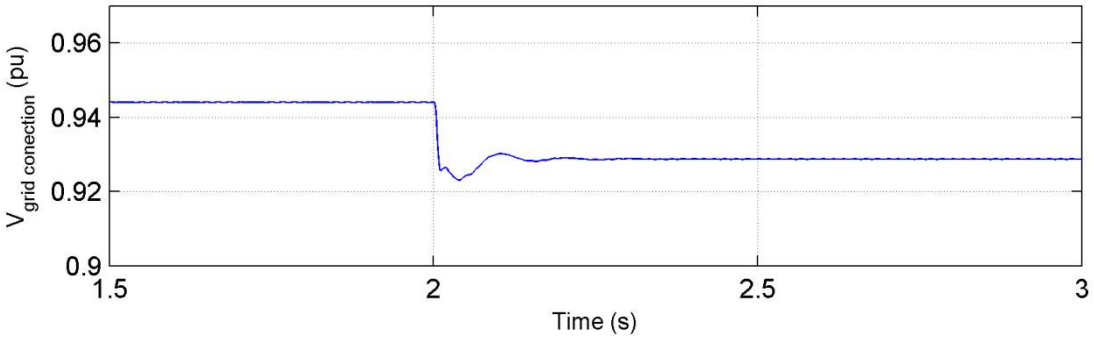

Fig. 5.5 Voltage on onshore grid connection during disconnection of the wind farm.

5.1.1 Influence of platform loads

Simulations are performed with different loads on the platforms to study the influence the platform load have on the system stability. Simulations on three load cases described in Table 4 are performed.

Table 4 Different platform load cases.

Load case 1: (Reference case)	50 % passive load, cos φ=1 40 % constant power load 10 % induction motor load
Load case 2:	40 % passive load, cos φ=1 40 % constant power load 20 % induction motor load
Load case 3:	50 % passive load, cos φ=0.9 40 % constant power load 10 % induction motor load

Fig. 5.6 shows that the platform loads have very little influence on the voltage on the busbar.

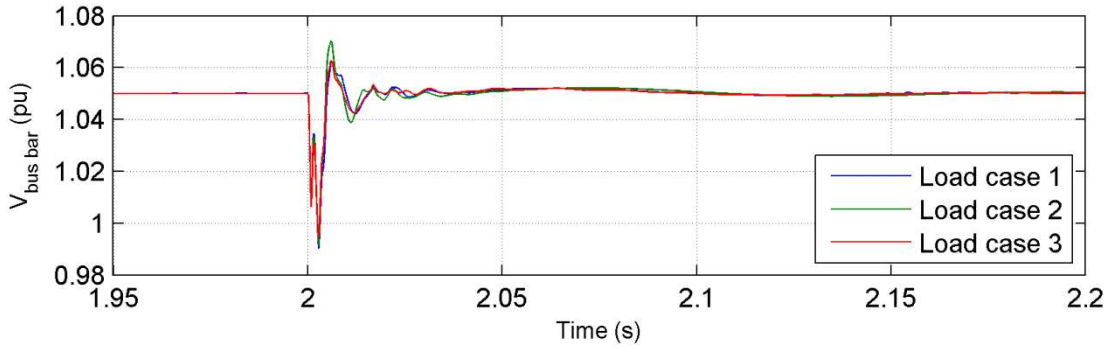

Fig. 5.6 Voltage on busbar during disconnection of the wind farm for different platform loads.

The voltage on platform 1 during disconnection of the wind farm for different platform loads is shown in Fig. 5.7. It can be noticed that the shape of the voltage are very similar but the amplitude is lower in load case 1 and 2 due to larger inductive load on the platform and hence larger voltage drop in the cable.

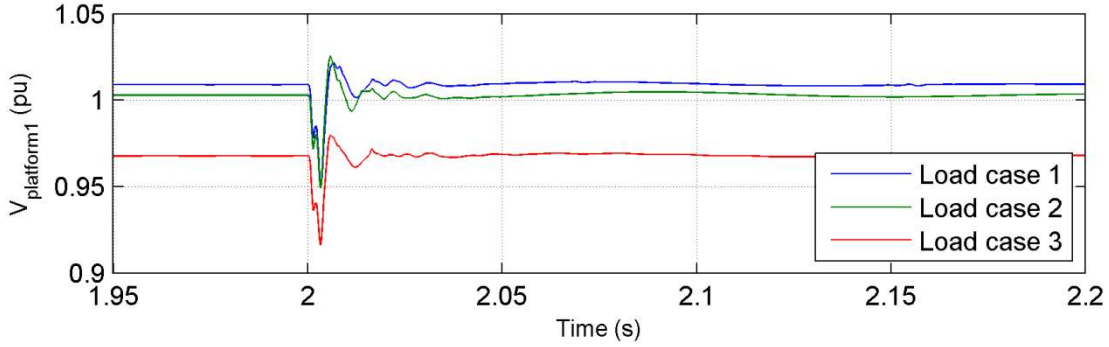

Fig. 5.7 Voltage on platform 1 during disconnection of the wind farm for different platform loads.

The active power from the offshore converter to the busbar is illustrated in Fig. 5.8. The increased share of induction motor load in load case 2 causes slightly larger oscillations in the power due to the speed oscillations in the motor. In load case 3 power oscillations between the increased inductive load on the platforms and the capacitances in the offshore cables introduce small fluctuations in the active power.

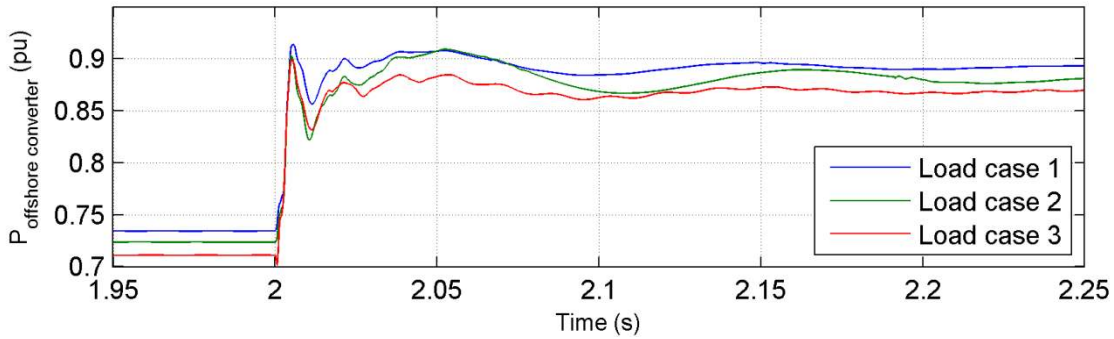

Fig. 5.8 Active power from offshore converter to busbar during disconnection of the wind farm for different platform loads.

5.1.2 Influence of offshore voltage controller

The control parameters on the offshore voltage controller are changed to make the response time of the controller twice as long. The simulation is then repeated to study the influence the offshore voltage controller have on the results. The voltage on the offshore terminals of the DC cable and the voltage on the busbar is shown in Fig. 5.9. The active power from the offshore converter to the busbar is shown in Fig. 5.10. It is seen that the slower offshore voltage controller have little influence on the dynamics of the system.

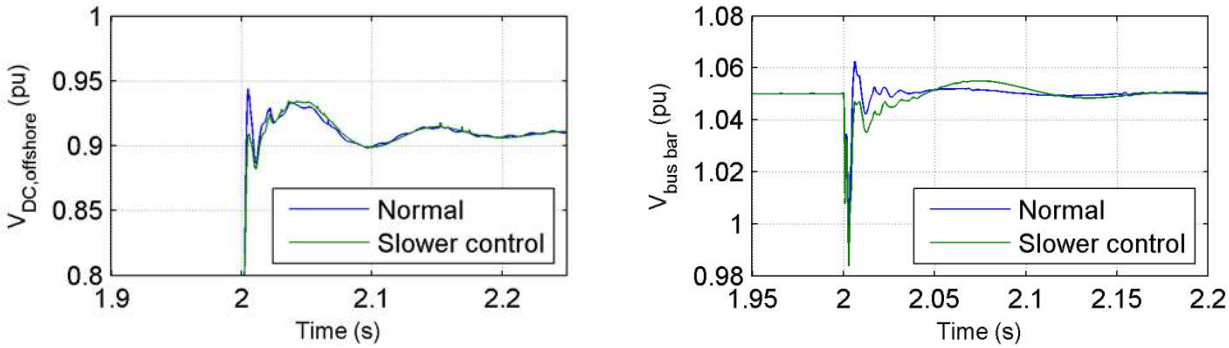

Fig. 5.9 a) Voltage on DC cable, and b) voltage on the offshore busbar during disconnection of the wind farm with different control parameters on the offshore voltage controller.

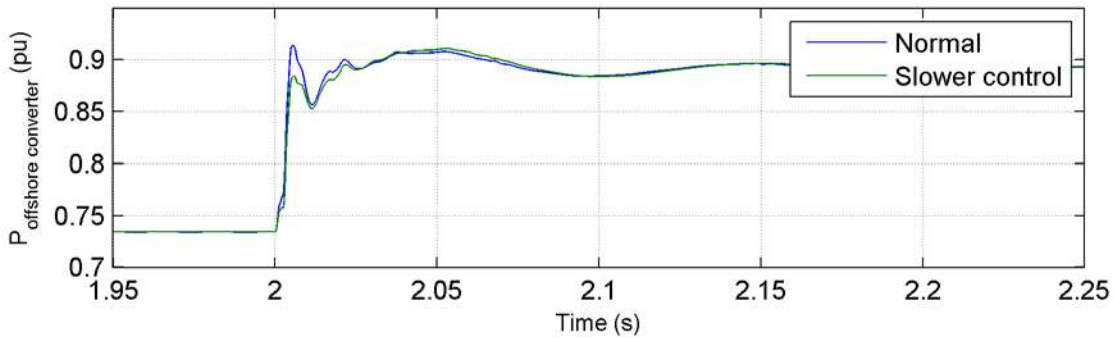

Fig. 5.10 Active power from offshore converter to the busbar during disconnection of the wind farm for different control parameters on the offshore voltage controller.

5.2 Start up of induction motor.

In this simulation an induction motor on 5 MW is started on platform 1. To reduce the start up time of the motor and hence the simulation time the inertia of the motor is set relatively low. This will not affect the transients except for making the motor accelerate faster. Similar transients may also be caused by starting several small induction motors at the same time. Large motors are usually equipped with a frequency converter to limit starting current and start up of this many small induction motors at the same time is not realistic in real life. The point of this simulation is to create a large disturbance in the system to see how the control system is able to respond and to determine the limitations associated with start up of large motors on the platforms. The motor are started at t=2 s. and the results of the simulations are shown in Fig. 5.11 - Fig. 5.14.

Fig. 5.11 shows the electromagnetic torque induced in the motor and the rotor speed during start up. The oscillations in the speed and torque just after the motor is connected and before the speed is stabilized at rated speed are the same as illustrated in Fig. 3.8.

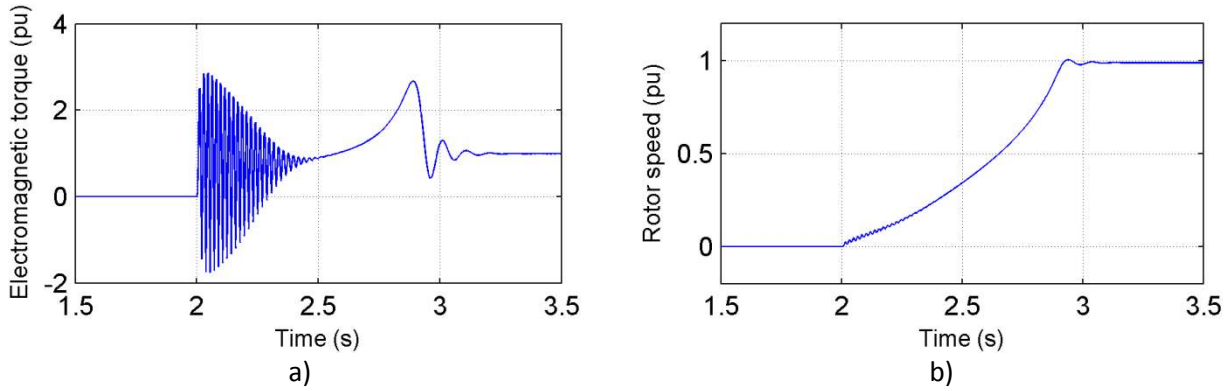

Fig. 5.11 a) Induced electromagnetic torque and b) rotor speed of motor during start up.

The active power flow in the system is shown in Fig. 5.12. The oscillations in the motor torque and speed cause the power from the onshore power grind, through the DC cable and the offshore converter to oscillate during acceleration of the motor. It is seen that the control strategy is working as intended and the HVDC transmission system handles the disturbance while the active power from the wind farm remains virtually unaffected by the motor start up.

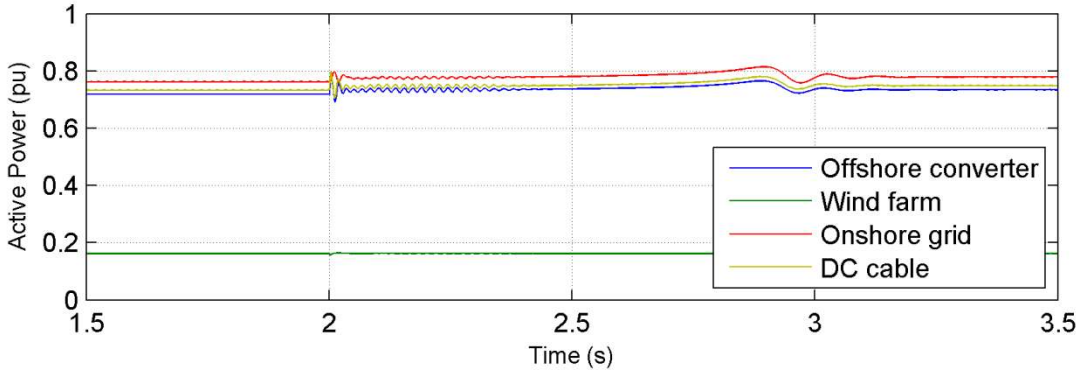

Fig. 5.12 Active power flow during motor start up on platform 1.

The voltages in the system are shown in Fig. 5.13. There is a negative peak on 0.03 pu in the busbar voltage caused by the large inrush current in the motor but the voltage is quickly reestablished. There are also some small oscillations when the motor reaches its operational speed and the motor current is reduced. These fluctuations can also be seen in the DC cable voltage. Because of the large starting current in the motor the voltage on platform 1 drops during acceleration of the motor. The voltage on the platform is however within the limitations stated in Table 3. The DC link voltage in the wind turbine converter is practically unaffected by the motor start up.

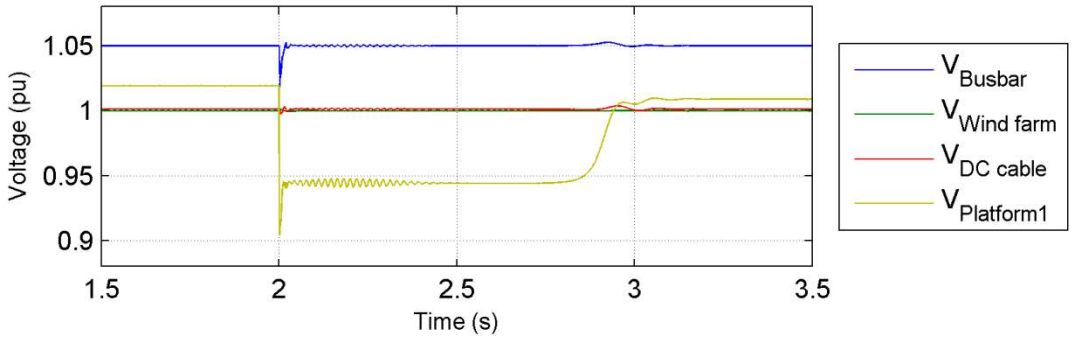

Fig. 5.13 Voltages in the system during motor start up on platform 1.

Fig. 5.14 shows the apparent-, active-, and reactive power from the offshore converter into the busbar. The reactive power generated by the cables exceeds the reactive power consumed by the platforms during normal operations, so when the motor is started the reactive power flow in the offshore converter is reduced. The increase in active power is small compared to the reduction in reactive power so the apparent power from the offshore converter is reduced during start up of the motor.

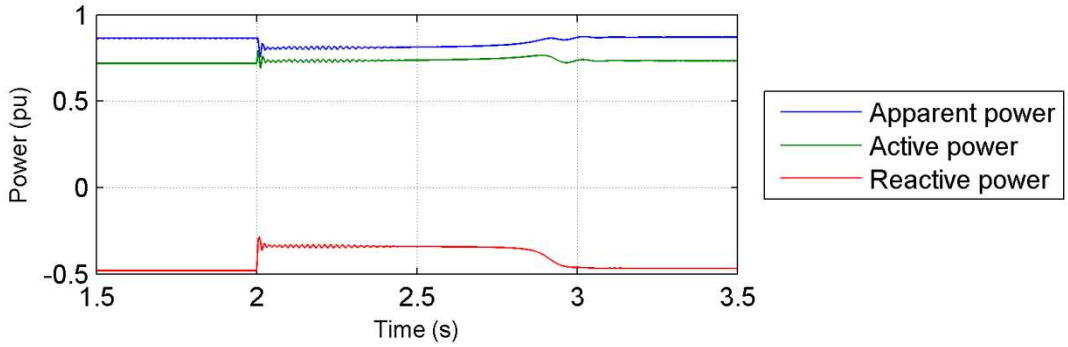

Fig. 5.14 Power from the offshore converter into the busbar during motor start up on platform 1.

5.2.1 Direct on line motor start up limitations.

In this section four motors with rating up to 30 MW are started on platform 1 to examine the limitations regarding direct on line start up of induction motors in this system.

Fig. 5.15 shows the apparent power from the offshore converter into the busbar. It can bee seen that the apparent power is below the rated value of the converter for all the motors tested in this simulation. This is because of the large reactive power generation of the offshore AC cables.

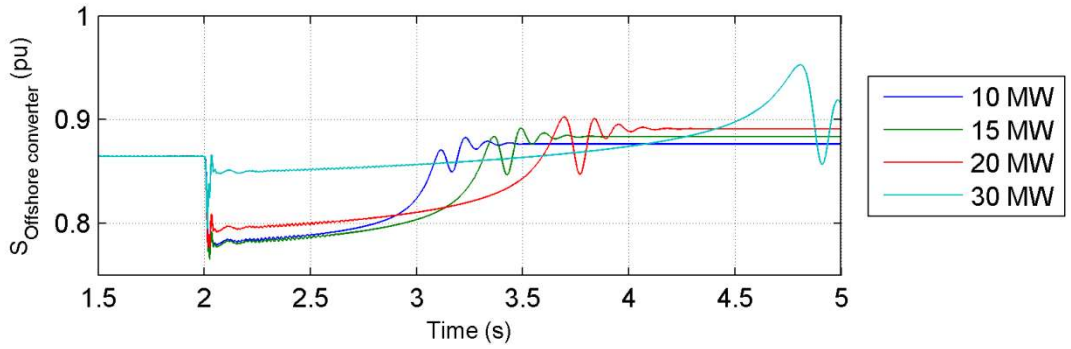

Fig. 5.15 Apparent power on offshore converter into the busbar during motor start up of different size induction machines.

To assure that the voltage drop on platform is minimized during start up of the motor, it is essential that the offshore voltage controller reacts quickly and brings the voltage on the offshore busbar back to its reference. Fig. 5.16 shows that the voltage on the busbar is reestablished after 0.04 s after connecting the 30 MW motor.

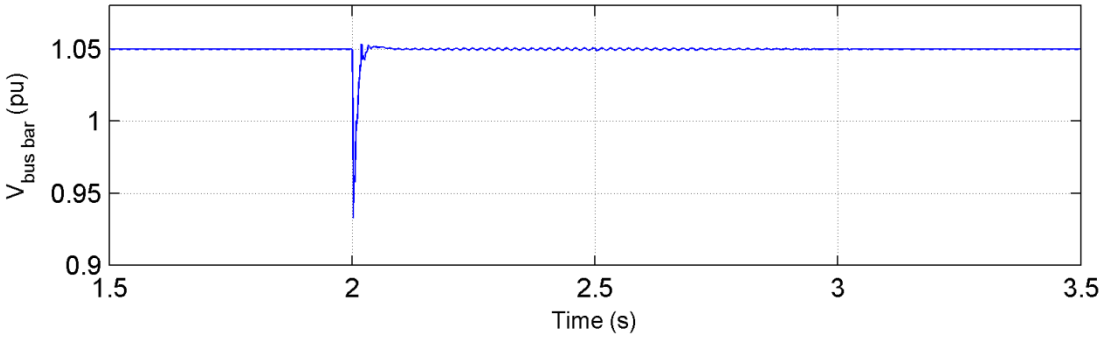

Fig. 5.16 Busbar voltage during start up of a 30 MW motor on platform 1.

The voltage on platform 1 is shown in Fig. 5.17. During start up of the 10 MW motor the voltage keeps within the limits given in Table 3, but for the larger motors the transient voltage variations exceeds the limitations given in the grid code. It is worth mentioning that the voltage on the platform is able to recover in all cases. It was not possible to start a larger motor because the platform voltage became to low and the motor did not have sufficient starting torque.

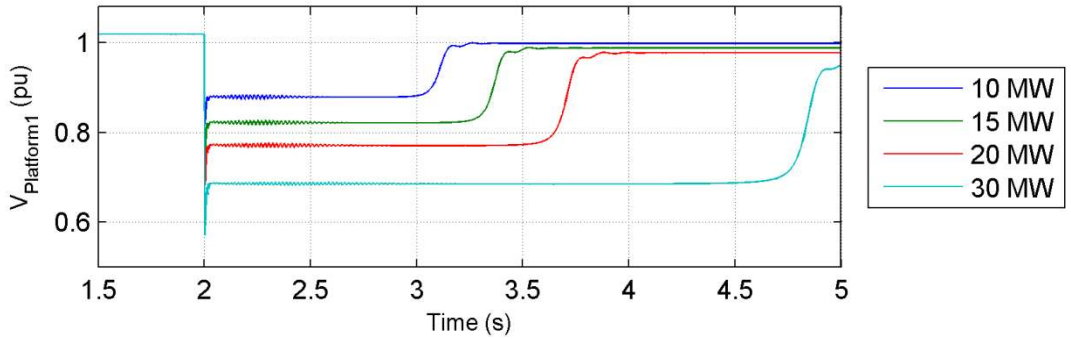

Fig. 5.17 Voltage on platform 1 during motor start up of different size induction machines on platform 1.

5.3 Dip in onshore power grid voltage

A sag in the onshore voltage can be caused by a short-circuit, start up of a large motor, energizing of a transformer, or sudden load variation in the onshore power grid. It is important that the control system is able to handle these types of disturbance so that a dip in the onshore voltage not affects the operation on the platforms. A voltage sag in the onshore power grid is simulated to study the effect this have on the offshore voltage. The onshore voltage is reduced from 1 pu to 0.8 pu at t=2, and increased back to 1 pu at t=2.1.

Fig. 5.18 shows the voltages in the system during a voltage sag in the onshore power grid. The sag in the onshore voltage causes a disturbance in the voltage on the offshore terminals of the DC cable but the voltage controller is quick to bring the voltage back to its reference. On the busbar the voltage disturbance is further damped due to the offshore voltage controller and the busbar voltage only change with +/- 0.004 pu. Consequently the voltage remains fairly constant on the platforms and the wind farm during the voltage sag. The voltage on platform 1 and the wind farm drops with less than 0.3 % and 0.1 % respectively. The two voltage spikes with a few milliseconds duration occurring at t=2.0 s. and t=2.1 s. are most likely due the power balance in the ideal VSC model and is not realistic.

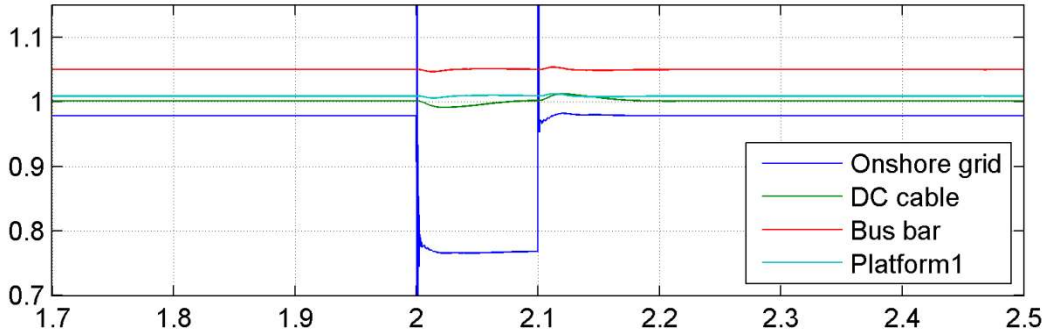

Fig. 5.18 Voltages in the system during voltage sag in onshore grid.

Fig. 5.19 shows the current from the onshore power grid to the onshore converter during the voltage sag on the onshore grid. It can be seen that the current exceeds 1 pu during the voltage drop. This is important to consider when dimensioning the onshore transformer and converter.

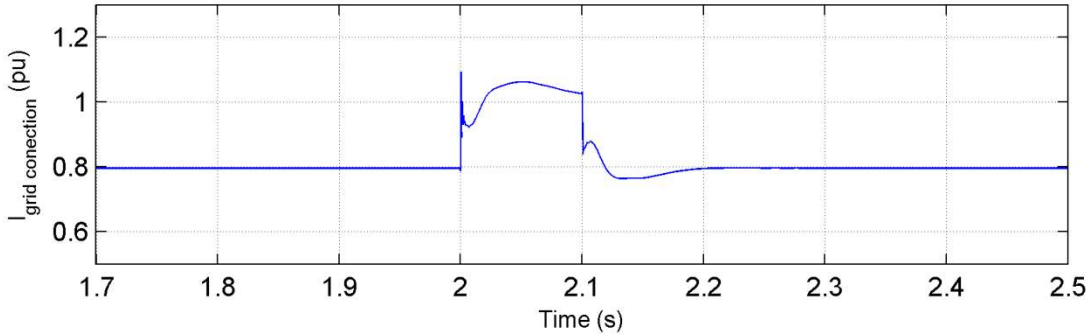

Fig. 5.19 RMS current from the onshore power grid to the onshore converter during a sag in the onshore voltage.

5.4 Load shedding.

During operation of an oil and gas platform situations may occur were parts of the load have to be disconnected. Components may fail causing large loads, or in worst case the whole platform, to trip. It is then important that a fault on one platform don't affect the operation on the other platforms in the power system. In this simulation case platform 2 is suddenly disconnected at t=2 s. to study the effect this has on the rest of the system.

Fig. 5.20 shows the voltages in the system during disconnection of platform 2. When the platform is disconnected the voltage on the busbar is increased. The offshore voltage controller reacts quickly to bring the voltage back to its reference. The voltage on the DC cable also rises before the onshore DC voltage controller reduces the active power into the cable. The voltage on the DC link in the wind farm is practically unaffected by the disturbance. It can be noticed that the voltage transients are almost exactly opposite to the voltages in Fig. 5.1 when the wind farm was disconnected.

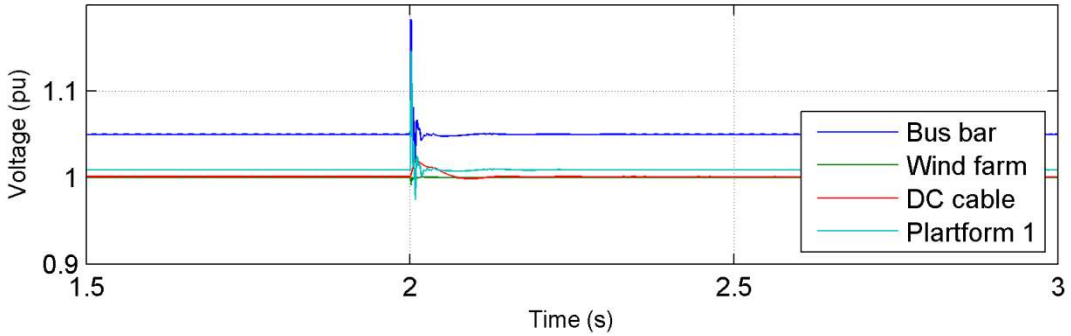

Fig. 5.20 Voltage in the system during disconnection of platform 2.

The active power flow in the system during disconnection of platform 2 is illustrated in Fig. 5.21. The power from the offshore converter is decreased to meet the new demand. As in Fig. 5.2 the oscillations in power from the onshore power grid is slightly higher than in the offshore converter due to the losses in the DC cable.

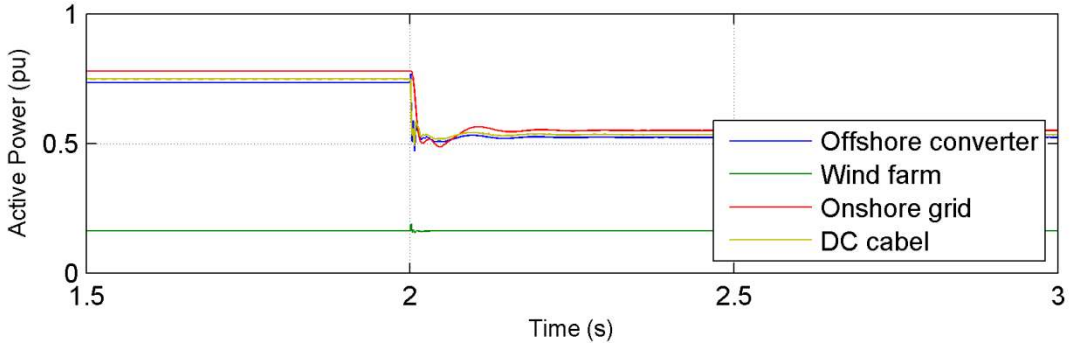

Fig. 5.21 Active power flow in the system during disconnection of platform 2.

5.4.1 Influence of cable model

Fig. 5.1 and Fig. 5.20 reveal spikes and rapid oscillations in the busbar voltage during sudden changes in the load. The number of PI-sections in the offshore cables is changed form 1 to 5 and the simulation of the case, disconnection of platform 2 is repeated in order to study the influence of the offshore cable model.

Fig. 5.22 shows that the peak in the voltage on the busbar is reduced in the case with 5 PI-sections.

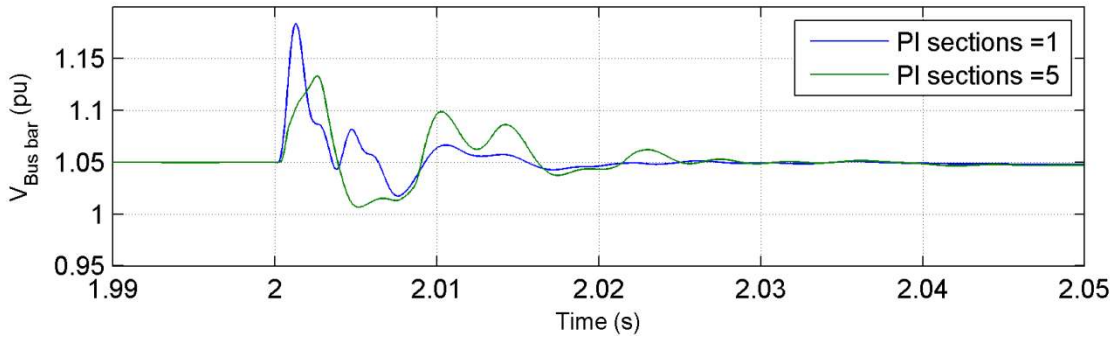

Fig. 5.22 Voltage on busbar during disconnection of platform 2 with different number of PI-sections on offshore cables.

5.4.2 Disconnect all platforms

Disconnection of all platforms at the same time is a highly unlikely event. However this is the largest load variation the control system can be exposed to and therefore a good way to test the model. The power transfer on the HVDC transmission system will then have to turn and power must start to flow into the onshore power grid since the wind farm is still producing power.

Fig. 5.23 shows the voltage on the busbar during disconnection of all platforms. There are some oscillations but the controller brings the voltage back to the reference after 0.05 s.

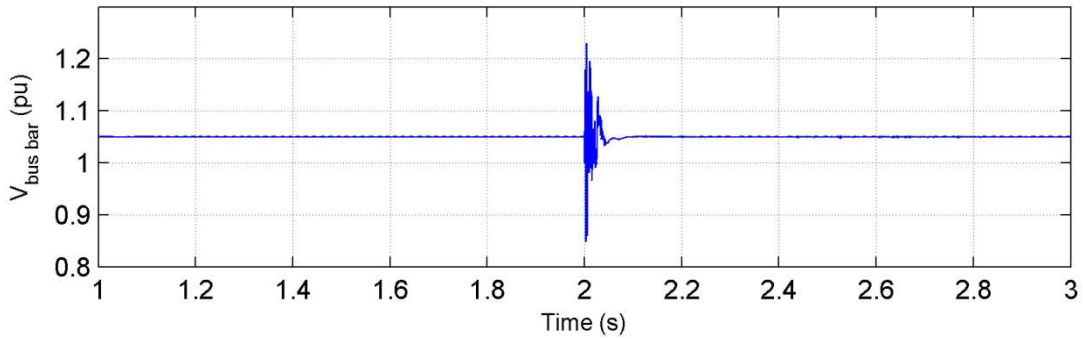

Fig. 5.23 Busbar voltage during disconnection of all platforms.

The active power from the offshore converter into the busbar is shown in Fig. 5.24. When the platforms are disconnected the direction of the power is changed and the power from the wind farm is transferred to shore.

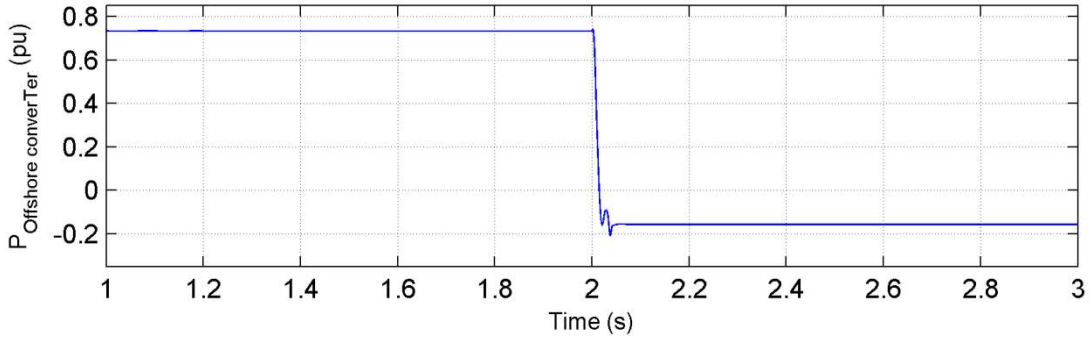

Fig. 5.24 Active power from the offshore converter to the busbar during disconnection of all platforms.

6 Discussion

The simulations show that the control system developed is working according to the control strategy. The onshore- and offshore- converter reacts quickly on changes in the voltage on the DC cable and the offshore busbar respectively. Consequently the VSC-HVSC transmission system is able to react quickly and adjust the delivered power according to changes in the demand on the offshore power grid. The wind farm controller is also able to keep the DC link voltage in the turbine back-to-back converter, and the rotational speed of the wind turbine practically constant during the disturbances. As a result the power production on the wind farm is virtually unaffected by the disturbances while the VSC-HVDC transmission assures stability in the system. The power oscillations from the wind farm are insignificant so the wind farm does not seem to have any negative effect on the operation on the platforms. The simulation results states that the control system was able to keep the voltage and frequency fluctuation on the platforms within the limits of the grid code [12] for all disturbances. Only during direct online start up of induction motors larger than 15 MW was the transient voltage drop in the platform to large. This was however due to the voltage drop in the cable and not the control system.

During start up of the induction motor on platform 1, the large starting current of the motor caused the voltage on the platform and the offshore busbar to drop. Fig. 5.16 shows that the VSC-HVDC control system was quickly able to restore the offshore busbar voltage to its reference even during start up of a 30 MW machine. The limitations regarding motor start up is therefore restricted to the voltage drop and the current rating of the AC cable. A slower controller would lead to a larger voltage drop on the platform during start up and herby limiting the rating of the motor possible to start direct online. The quick response of the offshore voltage controller is therefore considered very favorable regarding direct on line start up of induction motors on the platform.

The simulation results revealed some rapid oscillations in the voltage on the offshore busbar and hence the platforms at the moment of load shedding and tripping of the wind farm. See Fig. 5.1 and Fig. 5.20. Fig. 5.22 revealed that these voltage transients were affected by the cable model. The capacitance of the PI cable model will be directly connected to the offshore busbar. As a result a rapid change in the busbar voltage might cases a large current in the capacitances. The PI equivalent cable model is generally not well suited for fast transients and spurious oscillations generated by lumped parameter elements must be accepted [26]. Distributed parameter models or other model how take into account the frequency dependent parameters of the cable are usually more accurate. However they require shorter time steps and hence longer calculation time. To add a small inductor between the busbar and the PI model might also be enough the limit the oscillations.

Another possible explanation to the voltage oscillations might be errors in the calculation of the rms voltage. The breaker model used to disconnect the wind farm and the platform in the simulations are designed to open at current zero crossing. Thus the breaker uses approximately ½ voltage period to completely break the current. This is about the same duration as the voltage transients. The imbalance in the current before all three phases are interrupted, might cause fluctuations in the calculated rms voltage.

The simulations showed that a voltage sag in the onshore voltage only had a minor effect on the voltages in the offshore system due to the fast control on the VSC-HVDC transmission system. For a full AC transmission system the effect of a voltage sag as described in chapter 5.3 is believed to be far more dramatic. Due to difficulties concerning voltage regulation in an AC system the voltage on the offshore busbar would drop forcing the platform to reject much of its load, in order to restore the voltage, or even causing the power transmission system to trip due to over current.

The simulations are performed using an average VSC model witch has no time delay. A real converter will have a time delay given by the switching frequency of the converter. This time delay combined with other delays associated with a real life system will decrease the systems stability margins. The time delay of a VSC is however considered to be small. A detailed VSC model will also introduce harmonics in the AC voltage and ripple in the DC voltage but this will to a large extent be removed by filters. Overall it is not expected that the use of a detailed VSC model would have much effect on the results presented in this rapport.

In 5.1.2 it was showed that a slower response on the offshore voltage controller has very little effect on the simulation results. However the response of the slower offshore voltage controller in 5.1.2 was still relatively fast and any attempt to make the response time even slower caused the simulations to fail. It can therefore be assumed that the control parameters have some effect on the simulation results, but a more thorough sensitivity study is needed to determine the extent of this effect. The control parameters used in this study were obtained based on simulations and even though the results revealed a fast and accurate control, it is believed that more optimal parameters can be found making the control even faster. It is also possible to let the offshore wind farm contribute to support the voltage on the offshore busbar by providing dynamic reactive power. In sum this would in theory lead to a even more stable voltage on the offshore busbar.

The load on the platform varies greatly depending on which processes are running on the platforms and how the processes are designed. The simulation results revealed that a sudden change in the platform voltage caused the power drawn by the induction motors to oscillate. These oscillations will be affected by the motor parameters, and then especially the inertia of the rotor and the load. The motor power oscillations were however modest so the motor parameters are not believed to have a conspicuous effect on the systems stability. The sensitivity study also showed that the load on the platforms only has a minor influence on the results. The load model is therefore considered detailed enough and it is not believed that a more detailed model would have considerable effect on the simulation results.

There are some uncertainties regarding the frequency measurements. The simulations were performed using a discrete model with a sampling time of 50 μs. This may lead to an inaccuracy in the frequency measurement which can explain the static variation from the fundamental frequency shown in Fig. 5.3. The transient behavior is also uncertain because of the limited number of voltage periods during the transients. The oscillations in the frequency is believed to be changes in the voltage phase angle.

7 Conclusion and further work.

7.1 Conclusion

A hypothetical power system in the north sea have been studied in order to investigate whether this system configuration is a feasible way to integrate offshore wind power and oil and gas platforms to the onshore power grid. A dynamic simulation model of the system has been made. A control strategy and a VSC control system based on vector control have also been created.

It is concluded that the control system is working according to the control strategy. All the developed controllers are able to efficiently track there references even during large disturbances. The VSC-HVDC transmission system is capable of quickly adjusting the delivered power to meet changes in the offshore power demand, leaving the power production on the wind farm practically unaffected by the disturbances introduced to the system. The control system is also able to assure stable operation conditions for the oil and gas platforms during the disturbances simulated and the voltage and frequency oscillations are kept within the limits of the grid code. The system was exposed to, and able to handle, large and partly unrealistic disturbances, so it can be concluded that the system handles variations in the load very well.

The results of the simulations indicate that the system configuration reviewed in this thesis represent a feasible way to integrate oil and gas platforms and offshore wind power with the onshore power grid.

7.2 Further work

The simulation results presented in this paper indicate feasibility of the system configuration investigated in this study. However more detailed work needs to be done before a clear conclusion is made.

The simulations in this thesis are done using an average VSC model. This limits the transients it is possible to study. Simulations with a detailed VSC model including switches should be performed in order to study short circuits and other transients to fast to be investigated with an average VSC model.

The reactive power from the wind farm is in this rapport set to zero. Dynamic reactive power from the wind farm can be used to support the voltage on the offshore busbar. To investigate different ways to control the voltage on the offshore busbar and the effect of including dynamic reactive power control from the wind farm is recommended as future work.

This rapport only investigates one way to integrate oil and gas platforms and offshore wind power to the onshore power grid. Other system configurations should be investigated and the results should be compared in order to find the system configuration most suitable. The choice of configuration will however depend on a lot of things like: the number of platforms and wind farms and the distance between them, the distance from shore, and the investment cost. For instance if the distance between the offshore platforms is large, a multi terminal HVDC system might have certain advantages.

Bibliography

[1] Ministry of Environment, "regjeringen.no," [Online]. Available: http://www.regjeringen.no/nb/dep/md/tema/klima.html?id=1307. [Accessed 7 Nowenber 2012].

[2] Statistisk sentralbyrå, "ssb.no," [Online]. Available: https://www.ssb.no/en/natur-og-miljo/statistikker/klimagassn. [Accessed 7 5 2013].

[3] Oljedirektoratet, NVE, Petroliumstilsynet, Statens Forurensningstilsyn, "Power from shore the the Norwegian continental shelf (translated from Norwegian)," 2008.

[4] Norwegian Oil and Gas Association, "Environmental report," 25 June 2012. [Online]. Available: http://www.norskoljeoggass.no/en/Publica/Environmental-reports/. [Accessed 7 Nowember 2012].

[5] Klima- og forurensningsdriektoratet, NVE, Oljedirektoratet, Petroliumstilsynet, "Klimakur 2020 - Sektoriell tiltaksanalyse petroliumssketoren," 2010.

[6] the Ministry of Petroleum and Energy, "An industry for the future – Norway's petroleum activities. Meld. St. 28 (2010–2011) Report to the Storting (white paper)," regjeringen.no, Oslo, 2011.

[7] Sweco Grøner, "Potensialstudie av havenergi i Norge [Potential study of ocean energy in Norway]," 2007.

[8] H. Wei and e. al., "The Potential of Integrating Wind Power with Offshore," MULTI-SCIENCE PUBLISHING COMPANY, Bergen, 2010.

[9] H. G. Svendsen, M. Hadiya, E. V. Øyslebø and K. Uhlen, "Integration of offshore wind farm with multiple oil," IEEE, Trondheim, 2011.

[10] A. R. Årdal, "Feasibility Studies on Integrating Offshore Wind Power with Oil Platforms," Norwegian University of Science and Technology, 2011.

[11] M. E. Theisen, Ø. Rui and T. Gjengedal, "Stability Analysis of an Offshore Grid supplied by a HVDC-VSC," in *Proc. 2011 14th European Conference on Power Electronics and Applications*, Trondheim, 2011.

[12] IEC 61892, "Mobile and fixed offshore units –Electrical installations".

[13] A.-I. Stan and D. I. Stroe, "Control of VSC-Based HVDC Transmission System for Offshore Wind Power Plants," [Online].

[14] A. Yazdani and R. Iravani, Voltage-Sourced Converters in Power Systems, Hoboken: John Wiley &

Sons, Inc., 2001.

[15] Siemens, "HVDC PLUS – Basics and Principle of Operation," Siemens, 2008.

[16] S. J. Chapman, Electric Machinery Fundamentals, 4th ed, Singapore: McGraw Hill, 2005.

[17] ABB, "XLPE Submarine Cable Systems: Attachhment to XLPE Land Cable Systems - User's Guide," [Online]. Available: www.abb.com. [Accessed 16 11 2012].

[18] MathWorks, inc, "MathWorks Documentation center," [Online]. Available: http://www.mathworks.se/help/physmod/powersys/ref/windturbine.html?searchHighlight=wind+turbine. [Accessed 25 May 2013].

[19] MathWorks, inc, "MathWorks Documentation center," [Online]. Available: http://www.mathworks.se/help/physmod/powersys/ref/permanentmagnetsynchronousmachine.html?searchHighlight=permanent+magnet+synchronous+machine. [Accessed 30 April 2013].

[20] S. Frydenlund, *Lecture on Marine and offshore power systems,* Trondheim, 2012.

[21] C. P. Krause, O. Wasynczuk and S. D. Sudhoff, Analysis of electric machinery and drive systems, New York: IEEE Press, 2002.

[22] P. K. Kovács, Transient Phenomena in Electrical Machines, Amsterdam: Elsevier Science Publisher B. V., 1984.

[23] R. Song and e. al., "VSCs based HVDC and its control strategy," IEEE, 2005.

[24] C. Bajracharya, "Control of VSC-HVDC for windpower," Norwegian University of Science and Technology, Trondheim, 2008.

[25] N. Mohan, Advanced Electric Drives, Minneapolis: MNPERE, 2001.

[26] P. O. Hevia, "Alternative transients program - Comparison of transmission line models," iitree, Santa Fe.

Appendix

Appendix A: Base values for per unit representation

Sbase=300MVA

$V_{base} = V_n$ (nominal peak phase-to-ground voltage)

$$I_{base} = \frac{S_{base}}{V_{base}}$$

$$Z_{base} = \frac{V_{base}^2}{S_{base}}$$

Appendix B: Parameters

Onshore grid:

Phase-to-phase rms voltage	300 kV
Frequency	50 Hz
3-phase short circuit level	2500 MVA
X/R ratio	6

Grid impedance: $Z_G = \frac{U_G^2}{S_G} = \frac{300kV^2}{2500MVA} = 36\Omega$

Grid resistans: $R_G = \cos\phi \cdot Z_G = \cos(\tan^{-1} 6)) \cdot 36\Omega = 5.92\Omega$

Grid inductance: $L_G = \frac{6R_G}{2\pi f} = 0.113H$

Converter transformer:

Nominal power	300 MVA
Configuration	Yg,Yg
Frequency	50 Hz (Onshore transformer) 60 Hz (Offshore transformer)
Voltage ratio	$\frac{300kV}{120kV}$ (Onshore transformer) $\frac{120kV}{90kV}$ (Offshore transformer)
R1	0.0025 pu
R2	0.0025 pu
L1	0.075 pu
L2	0.075 pu
Rm	500 pu
Lm	500 pu

Phase reactor:

X_L	0.15 pu
R	0.01 pu

VSC-HVDC system:

$V_{DC,n}$(pole-to-pole)	240 kV
P_n	300 MVA
I_n	$\frac{P_n}{V_n} = \frac{300MVA}{240\ kV}$=1250A
C_{DC}	5.21µF

DC cable:

Length	220 km
Number of pi sections	2
Resistance	13.9 mΩ/km
Inductance	0.159 mH/km
Capacitance	0.231 µF/km

AC cables:

Number of pi sections	1
Resistance	99.1 mΩ/km
Inductance	0.46 mH/km
Capacitance	0.14 µF/km

Wind turbine:

Nominal mechanical output power	2 MW
Base wind speed	12 m/s
Maximum power at base wind speed	1 pu

PMSG:

Nominal power	2 MW
Stator phase resistance	0.015 Ω
Armature inductance	2.122 mH
Flux linkage established by magnets	4.814 V.s
Inertia	8000 kg*m^2
Pole pairs	40
Rotor type	Round

Control parameters:

Onshore controller		
Inner controller	Kp	2
	Ki	50
DC voltage controller	Kp	5
	Ki	200
Offshore controller		
Busbar voltage controller	Kp	0.1
	Ki	150
Wind farm generator side		
Inner controller	Kp	5
	Ki	50
Speed controller	Kp	10
	Ki	100
Wind farm grid side		
Inner controller	Kp	2
	Ki	50
Reactive power controller	Kp	0.5
	Ki	100
DC voltage controller	Kp	1
	Ki	1000
Pitch controller		
	Kp	5
	Ki	50
	Kw	3.33

Appendix C: MATLAB script

This scrip plots Cp-λ characteristic for the wind turbine model.

```
%plots Cp to lamda for the simulink wind turbine model for different pitch
%angles
for b=0:5:15
    hold on;
    la=0:0.1:15;
    la_i=1./((1./(la+0.08*b))-(0.035./(b^3+1)));
    Cp=0.5176.*((116./la_i)-(0.4.*b)-5).*exp(-21./la_i)+0.0065.*la;
    plot(la,Cp);
end
axis([0 15 -0.1 0.5]);
xlabel('\lambda');
ylabel('c_p');
grid;

b=0;
la=0:0.1:15;
la_i=1./((1./(la+0.08*b))-(0.035./(b^3+1)));
Cp=0.5176.*((116./la_i)-(0.4.*b)-5).*exp(-21./la_i)+0.0065.*la;
maxCp=max(Cp);
indexAtMax = find(Cp == maxCp);
xAtMax = la(indexAtMax);
x=[0 xAtMax];
y=[maxCp maxCp];
plot(x,y,'--');
plot([xAtMax xAtMax],[-0.1 maxCp],'--');
```

This script prints all simulation results to diff image files.

```
figure (1)
hFig = figure(1);
set(gcf,'PaperUnits','inches','PaperPosition',[0 0 6.52 1.85])

%Onshore grid conection
plot(gridcon.time,gridcon.signals(1,1).values(:,1));
xlabel('Time (s)','FontSize',9);
ylabel('V_g_r_i_d_ _c_o_n_e_c_t_i_o_n (pu)', 'FontSize',9);
axis([1.5 3.5 0.9 0.97]);
grid
print -dtiff -r300 Vgridcon;

plot(gridcon.time,gridcon.signals(1,2).values(:,1));
xlabel('Time (s)','FontSize',9);
ylabel('I_g_r_i_d_ _c_o_n_e_c_t_i_o_n (pu)', 'FontSize',9);
axis([1.5 3.5 0.7 0.9]);
grid
print -dtiff -r300 Igridcon;

plot(gridcon.time,gridcon.signals(1,3).values(:,1));
xlabel('Time (s)','FontSize',9);
```

```
ylabel('P_g_r_i_d_ _c_o_n_e_c_t_i_o_n (pu)', 'FontSize',9);
axis([1.5 3.5 0.7 0.9]);
grid
print -dtiff -r300 Pgridcon;

%DC cable offshore conection
plot(DCoffshore.time,DCoffshore.signals(1,1).values(:,1));
axis([1.5 3.5 0.6 0.9]);
xlabel('Time (s)','FontSize',9);
ylabel('I_D_C_,_o_f_f_s_h_o_r_e (pu)','FontSize',9);
grid;
print -dtiff -r300 Idcoffshore;

plot(DCoffshore.time,DCoffshore.signals(1,2).values(:,1));
axis([1.5 3.5 0.95 1.05]);
xlabel('Time (s)','FontSize',9);
ylabel('V_D_C_,_o_f_f_s_h_o_r_e (pu)','FontSize',9);
grid;
print -dtiff -r300 Vdcoffshore;

plot(DCoffshore.time,DCoffshore.signals(1,3).values(:,1));
axis([1.5 3.5 0.6 0.9]);
xlabel('Time (s)','FontSize',9);
ylabel('P_D_C_,_o_f_f_s_h_o_r_e (pu)','FontSize',9);
grid;
print -dtiff -r300 Pdcoffshore;

%Offshore bubar
plot(BB_IVPQ.time,BB_IVPQ.signals(1,1).values(:,1));
axis([1.5 3.5 0.7 0.9]);
xlabel('Time (s)','FontSize',9);
ylabel('I_b_u_s_ _b_a_r (pu)','FontSize',9);
grid;
print -dtiff -r300 Ibusbar;

plot(BB_IVPQ.time,BB_IVPQ.signals(1,2).values(:,1));
axis([1.5 3.5 1 1.08]);
xlabel('Time (s)','FontSize',9);
ylabel('V_b_u_s_ _b_a_r (pu)','FontSize',9);
grid;
print -dtiff -r300 Vbusbar;

plot(BB_IVPQ.time,BB_IVPQ.signals(1,3).values(:,1));
axis([1.5 3.5 0.7 0.8]);
xlabel('Time (s)','FontSize',9);
ylabel('P_b_u_s_ _b_a_r (pu)','FontSize',9);
grid;
print -dtiff -r300 Pbusbar;

plot(BB_IVPQ.time,BB_IVPQ.signals(1,4).values(:,1));
axis([1.5 3.5 -0.6 -0.2]);
xlabel('Time (s)','FontSize',9);
ylabel('Q_b_u_s_ _b_a_r (pu)','FontSize',9);
grid;
print -dtiff -r300 Qbusbar;
```

```
%Platform 1
plot(P4_IVPQ.time,P4_IVPQ.signals(1,1).values(:,1));
axis([1.5 3.5 0.15 0.35]);
xlabel('Time (s)','FontSize',9);
ylabel('I_p_l_a_t_f_o_r_m_1 (pu)','FontSize',9);
grid;
print -dtiff -r300 Iplatform1;

plot(P4_IVPQ.time,P4_IVPQ.signals(1,2).values(:,1));
axis([1.5 3.5 0.85 1.05]);
xlabel('Time (s)','FontSize',9);
ylabel('V_p_l_a_t_f_o_r_m_1 (pu)','FontSize',9);
grid;
print -dtiff -r300 Vplatform1;

plot(P4_IVPQ.time,P4_IVPQ.signals(1,3).values(:,1));
axis([1.5 3.5 0.15 0.45]);
xlabel('Time (s)','FontSize',9);
ylabel('P_p_l_a_t_f_o_r_m_1 (pu)','FontSize',9);
grid;
print -dtiff -r300 Pplatform1;

plot(P4_IVPQ.time,P4_IVPQ.signals(1,4).values(:,1));
axis([1.5 3.5 -0.1 0.4]);
xlabel('Time (s)','FontSize',9);
ylabel('Q_p_l_a_t_f_o_r_m_1 (pu)','FontSize',9);
grid;
print -dtiff -r300 Qplatform1;

Pbase=300e6;
Ptot=PQplatform.signals(1,1).values(:,1)/Pbase;
Pind=PQplatform.signals(1,2).values(:,1)/Pbase;
Pvsd=PQplatform.signals(1,3).values(:,1)/Pbase;
Ppassive=PQplatform.signals(1,4).values(:,1)/Pbase;
plot(PQplatform.time,Ptot,PQplatform.time,Pind,PQplatform.time,Pvsd,PQplatform
.time,Ppassive);
axis([1.5 3.5 -0.05 0.3]);
xlabel('Time (s)','FontSize',9);
ylabel('Active power. Platform1 (pu)','FontSize',9);
grid;

Qtot=PQplatform.signals(1,1).values(:,2)/Pbase;
Qind=PQplatform.signals(1,2).values(:,2)/Pbase;
Qvsd=PQplatform.signals(1,3).values(:,2)/Pbase;
Qpassive=PQplatform.signals(1,4).values(:,2)/Pbase;
plot(PQplatform.time,Qtot,PQplatform.time,Qind,PQplatform.time,Qvsd,PQplatform
.time,Qpassive);
axis([1.5 3.5 -0.05 0.]);
xlabel('Time (s)','FontSize',9);
ylabel('Reactive power. Platform1 (pu)','FontSize',9);
grid;


%Cable to platform 1
```

```
plot(P12_IVPQ.time,P12_IVPQ.signals(1,1).values(:,1));
axis([1.5 3.5 0.15 0.35]);
xlabel('Time (s)','FontSize',9);
ylabel('I_c_a_b_l_e_P_1 (pu)','FontSize',9);
grid;
print -dtiff -r300 IcableP1;

plot(P12_IVPQ.time,P12_IVPQ.signals(1,2).values(:,1));
axis([1.5 3.5 0.95 1.1]);
xlabel('Time (s)','FontSize',9);
ylabel('V_c_a_b_l_e_P_1 (pu)','FontSize',9);
grid;
print -dtiff -r300 VcableP1;

plot(P12_IVPQ.time,P12_IVPQ.signals(1,3).values(:,1));
axis([1.5 3.5 0.2 0.5]);
xlabel('Time (s)','FontSize',9);
ylabel('P_c_a_b_l_e_P_1 (pu)','FontSize',9);
grid;
print -dtiff -r300 PcableP1;

plot(P12_IVPQ.time,P12_IVPQ.signals(1,4).values(:,1));
axis([1.5 3.5 -0.2 0.2]);
xlabel('Time (s)','FontSize',9);
ylabel('Q_c_a_b_l_e_P_1 (pu)','FontSize',9);
grid;
print -dtiff -r300 QcableP1;

%wind farm
plot(wind.time,wind.signals(1,1).values(:,1));
axis([1.5 3.5 0.98 1.02]);
xlabel('Time (s)','FontSize',9);
ylabel('V_D_C_,_w_i_n_d_ _f_a_r_m (pu)','FontSize',9);
grid;
print -dtiff -r300 VDCwind;

plot(wind.time,wind.signals(1,2).values(:,1));
axis([1.5 3.5 0.7 1.3]);
xlabel('Time (s)','FontSize',9);
ylabel('I_D_C_,_w_i_n_d_ _f_a_r_m (pu)','FontSize',9);
grid;
print -dtiff -r300 IDCwind;

plot(wind.time,wind.signals(1,3).values(:,1));
axis([1.5 3.5 0.6 1.3]);
xlabel('Time (s)','FontSize',9);
ylabel('P_D_C_,_w_i_n_d_ _f_a_r_m (pu)','FontSize',9);
grid;
print -dtiff -r300 PDCwind;

plot(wind.time,wind.signals(1,4).values(:,1));
axis([1.5 3.5 0.98 1.02]);
xlabel('Time (s)','FontSize',9);
ylabel('\omega_t_u_r_b_i_n_e (pu)','FontSize',9);
grid;
print -dtiff -r300 wturbine;
```

```
%Motor
plot(motor.time,motor.signals(1,1).values(:,1));
axis([1.5 3.5 -500 2000]);
xlabel('Time (s)','FontSize',9);
ylabel('Rotor speed (rpm)','FontSize',9);
grid;
print -dtiff -r300 nmotor;

plot(motor.time,motor.signals(1,2).values(:,1));
axis([1.5 3.5 -1500 2000]);
xlabel('Time (s)','FontSize',9);
ylabel('Electromagnetic torque (N*m)','FontSize',9);
grid;
print -dtiff -r300 Temotor;

Te_base=110.31e3/(60*pi);
Te_pu=motor.signals(1,2).values(:,1)/Te_base;
n_pu=motor.signals(1,1).values(:,1)/(1800);

plot(motor.time,n_pu);
axis([1.5 3.5 -0.2 1.2]);
xlabel('Time (s)','FontSize',9);
ylabel('Rotor speed (pu)','FontSize',9);
grid;
print -dtiff -r300 nmotor_pu0;

plot(motor.time,Te_pu);
axis([1.5 3.5 -2 4]);
xlabel('Time (s)','FontSize',9);
ylabel('Electromagnetic torque (pu)','FontSize',9);
grid;
print -dtiff -r300 Temotor_pu0;

%Frequency
plot(freq.time,freq.signals(1,1).values(:,1));
axis([1.5 3.5 59.75 60.05]);
xlabel('Time (s)','FontSize',9);
ylabel('f_b_u_s_ _b_a_r (Hz)','FontSize',9);
grid;
print -dtiff -r300 Fbusbar;

plot(freq.time,freq.signals(1,2).values(:,1));
axis([1.5 3.5 49.7 50.1]);
xlabel('Time (s)','FontSize',9);
ylabel('f_o_n_s_h_o_r_e_ _c_o_n_v_e_r_t_e_r (Hz)','FontSize',9);
grid;
print -dtiff -r300 Fgrid;

%power
Pw=wind.signals(1,3).values(:,1)*50/300;
plot(BB_IVPQ.time,BB_IVPQ.signals(1,3).values(:,1),wind.time,Pw,gridcon.time,g
ridcon.signals(1,3).values(:,1),DCoffshore.time,DCoffshore.signals(1,3).values
(:,1));
axis([1.5 3 0 1]);
```

```
xlabel('Time (s)','FontSize',9);
ylabel('Active Power (pu)','FontSize',9);
grid;
print -dtiff -r300 activepower2;

plot(BB_IVPQ.time,BB_IVPQ.signals(1,4).values(:,1),P4_IVPQ.time,P4_IVPQ.signal
s(1,4).values(:,1));
axis([1.5 3.5 -0.5 0.5]);
xlabel('Time (s)','FontSize',9);
ylabel('Rective Power (pu)','FontSize',9);
grid;
print -dtiff -r300 reactivepower;

S_offc=sqrt(BB_IVPQ.signals(1,3).values(:,1).^2+BB_IVPQ.signals(1,4).values(:,
1).^2);
plot(BB_IVPQ.time,S_offc,BB_IVPQ.time,BB_IVPQ.signals(1,3).values(:,1),BB_IVPQ
.time,BB_IVPQ.signals(1,4).values(:,1));
axis([1.5 3.5 -0.5 1]);
xlabel('Time (s)','FontSize',9);
ylabel('Power (pu)','FontSize',9);
grid;
print -dtiff -r300 apparentpower;

%voltage
plot(BB_IVPQ.time,BB_IVPQ.signals(1,2).values(:,1),wind.time,wind.signals(1,1)
.values(:,1),DCoffshore.time,DCoffshore.signals(1,2).values(:,1),P4_IVPQ.time,
P4_IVPQ.signals(1,2).values(:,1));
axis([1.5 3 0.8 1.2]);
xlabel('Time (s)','FontSize',9);
ylabel('Voltage (pu)','FontSize',9);
grid;
print -dtiff -r300 systemvoltage;
```

Appendix d: Simulation model

Complete model:

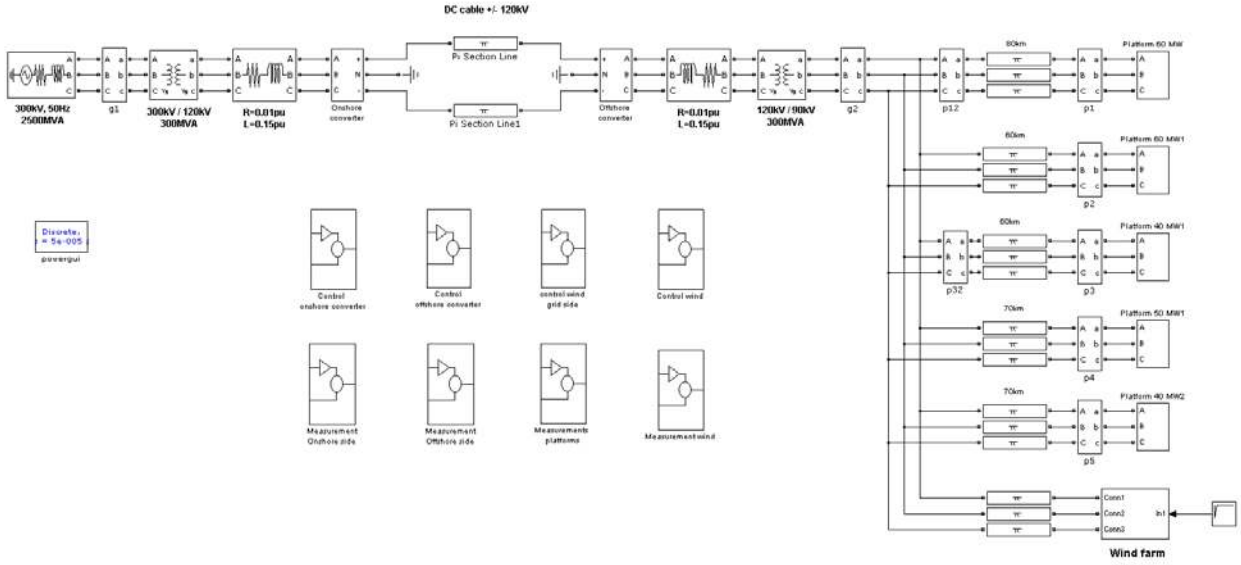

Wind farm:

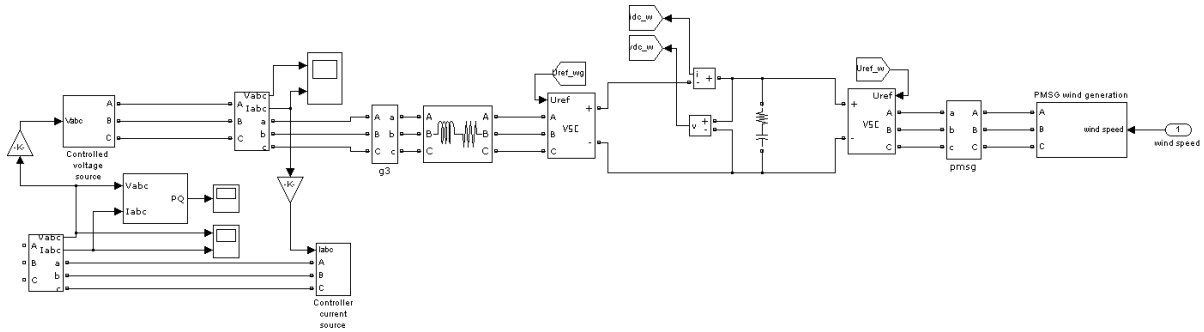

Converter model

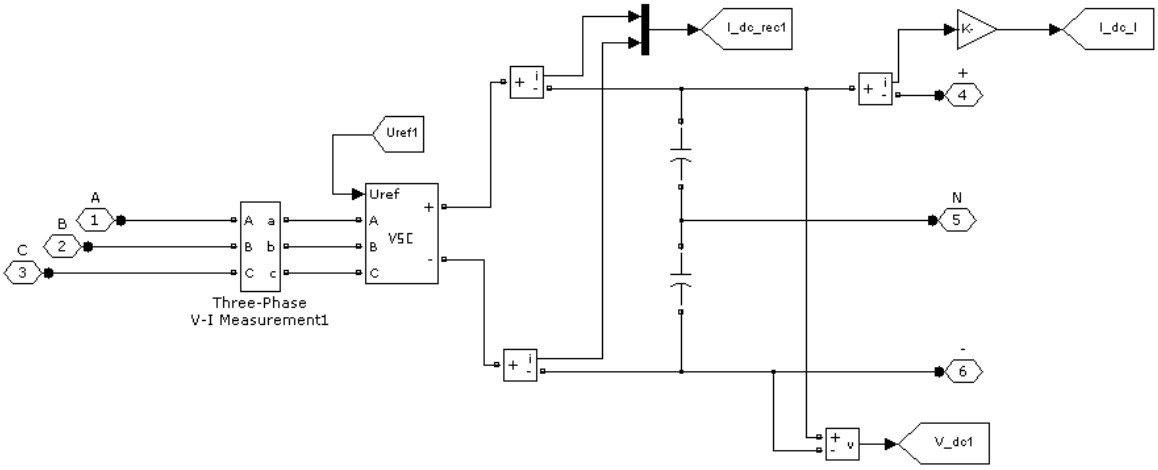

Onshore controller:

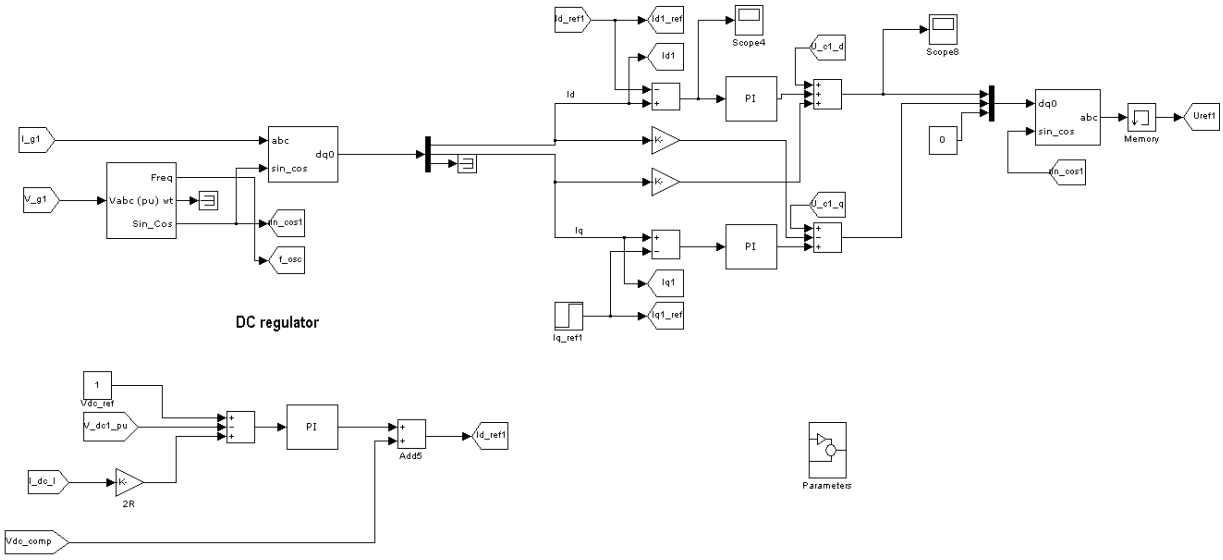

Offshore controller:

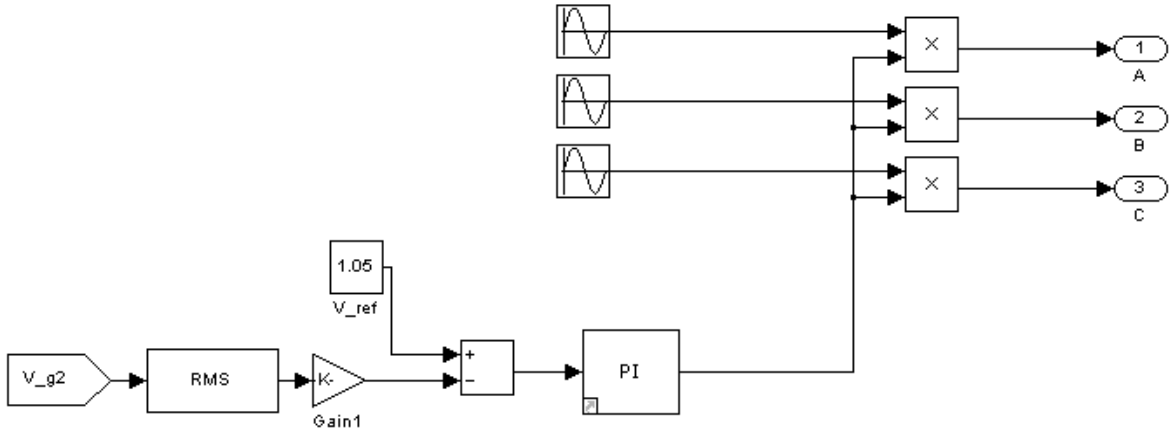

Wind farm grid side controller:

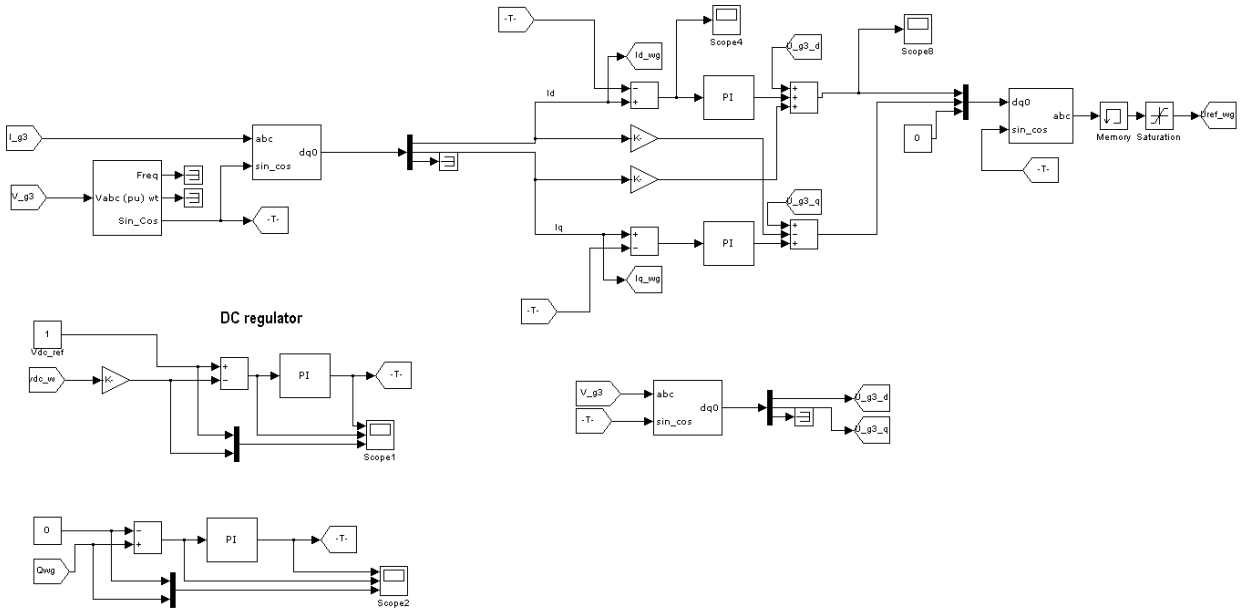

Wind farm generator side controller: